



Incorporation and substitution of ions and H₂O in the structure of beryl

Carina Silke Hanser^{1,2}, Tobias Häger^{1,2}, and Roman Botcharnikov^{1,2}

¹Institute of Geosciences, Johannes Gutenberg University Mainz,
J.-J.-Becher-Weg 21, 55099 Mainz, Germany

²Institute of Gemstone Research, Prof.-Schlossmacher-Straße 1, 55743 Idar-Oberstein, Germany

Correspondence: Carina Silke Hanser (chanser@uni-mainz.de)

Received: 21 November 2023 – Revised: 23 March 2024 – Accepted: 9 April 2024 – Published: 10 June 2024

Abstract. Incorporation of ions into the crystal structure of beryl (Be₃Al₂[Si₆O₁₈]) can take place by direct ion-to-ion substitution of the framework components Al³⁺, Be²⁺ and Si⁴⁺ or by occupation of interstitial or structural channel sites. The most common impurities in beryl include transition metals, alkalis and H₂O. It is accepted that the transition metals Mn, Cr and V directly substitute for Al at the octahedral site and induce colour. Similarly, the octahedral site can host Fe instead of Al. Nevertheless, it is shown that it remains disputed whether Fe can also be present at the tetrahedral, interstitial, or channel sites, and opposing hypotheses exist regarding these possibilities. However, in the case of Fe, not only the possible occupation of these sites remains under debate, but also their influence on the subsequent colour of beryl. Similarly, the residence of Li in the channels and at the Be tetrahedral or interstitial tetrahedral sites is still under debate. The presence of more than two types of H₂O (type I and type II) in the structural channels of beryl is also unclear. This article aims to give an overview on the consensus and on the current debates found in the literature regarding these aspects. It mainly concentrates on the substitution by and the role of Fe ions and on channel occupancy by H₂O.

1 Introduction

Beryl crystals (Be₃Al₂[Si₆O₁₈]) are often found in pegmatites, hydrothermal veins and schists. In particular, pegmatite-related beryl minerals are known for their large size and well-developed hexagonal, prismatic habit. This not only makes them attractive for mineral collectors, but also for petrologists as features such as growth zoning, inclusions and other impurities in these crystals can provide key information about growth conditions (e.g. Hawthorne and Černý, 1977; Charoy et al., 1996; Uher et al., 2012; Karamelas et al., 2019). In addition, the family of beryl comprises many coloured varieties (Table 1), making them popular gemstones, such as heliodor (yellow to greenish yellow), golden beryl (golden), morganite (pink to orange-pink), emeralds (green), red beryl (red to magenta) and aquamarine (blue to green-blue). In fact, emerald is one of the most important gemstones in the gemstone industry (Bersani et al., 2014; Groat and Turner, 2022; Khaleal et al., 2022; Mokhtar et al., 2023) and comes third after diamond and ruby in terms

of value (Groat et al., 2008). The colours of beryl are rooted in the incorporation of transition metal ions, such as Cr or V, into the structure of beryl. The constituting components of the beryl structure (Al, Si, Be) can directly be replaced by metal ions via isomorphic ion-to-ion substitution. Yet, the crystal framework of beryl also comprises open structural channels that are large enough to provide sufficient space to be occupied by larger ions, such as Ca, K and Cs, or molecules like H₂O. There has been a wide range of studies on the different beryl varieties in the past decades, especially with regard to colour-inducing metal ions and processes, as well as the presence of alkalis and H₂O in beryl. Some results have been reproduced by several studies and are thus widely accepted. However, there is still much debate regarding some colour-causing metal ions and the crystallographic positions they could be found at inside the beryl structure. This especially applies to Fe ions and the colours ranging between yellow and blue, which are thought to be induced by Fe impurities. In the case of the alkalis, the positions that

Li may occupy are similarly disputed. Likewise, the presence of various types of H₂O and the interactions of these molecules with other ions and the beryl structure itself have been a major concern of research in the past. Determining and understanding spectral features in beryl may also be essential for other areas of research since the importance of this mineral extends beyond the geosciences as well. The structure of beryl, with its open channels, makes it interesting for the field of electronics (Belyanchikov et al., 2017) and quantum mechanics computing (Mashkovtsev and Thomas, 2005). In addition, the characteristics and behaviour of H₂O molecules within its channels may allow for further deductions to be made that may also be applicable to more complex, biological systems involving interactions with nano-confined H₂O (Belyanchikov et al., 2017). This work aims to give an overview of the consensus and the current debates found in the beryl literature, especially regarding Fe ions and channel occupancy by H₂O.


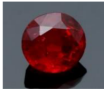







1.1 Crystal structure and chemistry

Beryl (Be₃Al₂[Si₆O₁₈]) is hexagonal, and its structure is described in the space group *P6/mcc* (e.g. Bragg and West, 1926; Blak et al., 1982; Pecherskaya et al., 2003; Gatta et al., 2006; Andersson, 2013; Lin et al., 2013; Fridrichová et al., 2015). However, cases of biaxiality in beryl have been reported (Goldman et al., 1978). The lengths of the unit cell edges along the axes *a* and *c* are also variable. They have been reported to be 9.21 and 9.17 Å, respectively (Bragg and West, 1926; Blak et al., 1982), while other authors give ranges of 9.210 to 9.245 Å along *a* and 9.190 to 9.220 Å along *c* (de Almeida Sampaio Filho et al., 1973) for natural beryls. Synthetic beryls have been shown to exhibit similar lengths of 9.2088 Å along *a* and 9.1896 Å along *c* (Morosin, 1972). The resulting unit cell of beryl contains two Be₃Al₂[Si₆O₁₈] formula units (Dvir and Low, 1960; Andersson, 2019). The crystal structure (Fig. 1) is characterised by interlinked Be-centred tetrahedra, Al-centred octahedra and Si-centred tetrahedra. As the latter combine to form hexagonal rings perpendicular to the *c* axis, they determine beryls as ring silicates or cyclosilicates (Mittani et al., 2002a; Viana et al., 2002a; Fridrichová et al., 2015; Skvortsova et al., 2015; Yu et al., 2017). Yet, beryl is sometimes also considered a tectosilicate in accordance with the classification by Zoltai, who interpreted the beryl structure as a three-dimensionally interlinked network of polyhedra (Zoltai, 1960; de Almeida Sampaio Filho et al., 1973; Aurisicchio et al., 1988). The Si tetrahedra rings are linked to each other via the Al octahedra and Be tetrahedra. While the Be tetrahedra and the Al octahedra share edges, the Si tetrahedra only share corners, both with the other polyhedra and among each other. Successive layers of this combination of polyhedra create channels parallel to the *c* axis of the hexagonal crystal structure. The channels have a maximum width of 5.1 Å (0.51 nm) (Kolesov and Geiger, 2000; Krambrock et al., 2002; Mashkovtsev et

al., 2016; Fukuda and Shinoda, 2008; Blak et al., 1982) alternating with bottlenecks of 2.8 Å (0.28 nm) (Kolesov and Geiger, 2000; Mashkovtsev et al., 2016; Blak et al., 1982; Fukuda et al., 2009), thus creating two possible crystallographic positions, referred to as *2a* and *2b* (Hawthorne and Černý, 1977; Aurisicchio et al., 1988; Mashkovtsev and Lebedev, 1993; Artioli et al., 1995; Fukuda and Shinoda, 2008; Mashkovtsev et al., 2016; Andersson, 2019) at the coordinates (0, 0, 0.25) for the *2a* site and (0, 0, 0) for the *2b* site, respectively (Hawthorne and Černý, 1977; Kolesov and Geiger, 2000; Aurisicchio et al., 1988; Fukuda and Shinoda, 2008; Artioli et al., 1995; Gatta et al., 2006; Fridrichová et al., 2018). In addition to the replacement of constituting ions by ions of similar valence state and radii as is possible in many minerals, the large dimension of the Si tetrahedra channels in beryl provides space for various large molecules and ions, such as H₂O or Na, K, Ca, and Cs, to be incorporated (Krambrock et al., 2002; Kolesov and Geiger, 2000). The alkali cations in the channels compensate for deficiencies in positive charges rooted in the ion-to-ion substitution of Al, Be or Si by ions of lower valence states (Aurisicchio et al., 1988; Fridrichová et al., 2018; Andersson, 2019). The presence of charged ions, in turn, causes electrostatic interactions with the dipole moment of the H₂O molecules in the channels. Therefore, H₂O molecules in beryl can be uncoordinated or coordinated with cations and are thus distinguished as type I and type II H₂O, respectively (e.g. Wood and Nassau, 1967; Kolesov and Geiger, 2000; Fukuda and Shinoda, 2008; Bidny et al., 2011; Mashkovtsev et al., 2016). This is discussed in more detail in the sections further below. Although alkalis and H₂O can be present, they are not generally mentioned in the chemical formula of beryl (Mihalynuk and Lett, 2003; McMillan et al., 2006; McManus et al., 2008).

The beryl group comprises many different chemically and structurally similar minerals with a primarily hexagonal crystal symmetry, alongside the name-giving beryls (Be₃Al₂[Si₆O₁₈]) themselves. The majority of these minerals is consistent with the general formula O₂T'₃T''₆X₁₈, with the positions being occupied by metal ions (O), Be (T'), Si (T'') and O (X), respectively (Pecherskaya et al., 2003). The other minerals in the beryl group include the Be-bearing pezzottaite (Cs(Be₂Li)Al₂Si₆O₁₈), bazzite (Sc₂Be₃Si₆O₁₈) and stoppaniite (Fe₂Be₃Si₆O₁₈) (Pecherskaya et al., 2003; Jehlička et al., 2017; Laurs et al., 2003; Pieczka et al., 2016). Furthermore, sekaninaite (Fe₂Al₄Si₅O₁₈) and indialite (Mg₂Al₄Si₅O₁₈) are regarded as members of this mineral group (Pecherskaya et al., 2003; Pieczka et al., 2016). While beryls themselves can be synthesised, synthetic compounds within the Mg₂Al₄Si₅O₁₈ – Mg₂BeAl₂Si₆O₁₈ and Mg₂Al₄Si₅O₁₈ – Mg₃Al₂Si₆O₁₈ series with beryl-like structures have also been produced (Pecherskaya et al., 2003). The orthorhombic, low-temperature polymorph of indialite is the mineral cordierite, which is also isostructural with beryl (Goldman et al., 1978; Aines and Rossman, 1984; Kolesov and Geiger, 2000). Hence, cordierite is often used as a refer-

Table 1. General information on and examples of the beryl varieties.

Variety	Morganite	Red beryl	Aquamarine	Heliodor	Golden beryl	Emerald	Goshenite
Example			 	 			
Colour	pink to orangey pink	red to magenta	blue to bluish green	yellow to greenish yellow	golden	yellowish green to bluish green	colourless
Main colouring element	Mn	Mn	Fe	Fe	Fe	Cr and/or V	none
Occurrence	granites, pegmatites, hydrothermal veins	rhyolite	granites, pegmatites, hydrothermal veins	pegmatites, hydrothermal veins	pegmatites, hydrothermal veins	pegmatites, hydrothermal veins, shales, rarely in granite	granite, pegmatites, hydrothermal veins

Photos by Qi Wang and Tom Stephan, German Gemmological Association, Idar-Oberstein, Germany.

ence material when assigning unknown absorption bands for the most common vibrational spectroscopies in beryl (Goldman et al., 1978). However, not all members of the beryl group are isostructural with beryl since pezzottaite, for instance, is not (Lambruschi et al., 2014).

1.2 Genesis of beryls

While Al and Si are major components of the continental crust of the Earth, Be is less abundant (Rudnick and Gao, 2003; Groat et al., 2008; Khaleal et al., 2022). Rudnick and Gao (2003) report 66.6 wt % for SiO₂ and 15.6 wt % for Al₂O₃ in the upper crust but only 2.1 ppm for Be. Though Be is a lithophile (Khaleal et al., 2022), it is incompatible in most silicate minerals (Hawthorne and Huminicki, 2002). This makes it possible for Be to become concentrated via fractionation processes leading to the crystallisation of its own mineral, beryl (Hawthorne and Huminicki, 2002). Beryl can be found in a variety of geological settings associated with rocks of the continental crust (Groat et al., 2008). These include pegmatitic, magmatic and metamorphic occurrences (Groat and Turner, 2022). Beryls associated with pegmatites are often found concentrated in pockets and cavities (Fig. 2). Those of magmatic origin can either form as non-concentrated, accessory minerals or in cavities within the cooling magma or by hydrothermal fluids interacting with the magmatic intrusion (Groat and Turner, 2022). Beryl can also form when Be-rich rocks are exposed to temperature and pressure changes. This results in metamorphism, a solid state process in which those mineral phases originally stable in the rock transform into mineral phases (including beryl), which are more stable under the altered conditions (Groat and Turner, 2022). The majority of beryls can be found in pegmatites and hydrothermal veins alongside with

other minerals such as feldspars, quartz or topaz (Jehlička et al., 2017; Viana et al., 2002b; Nassau and Wood, 1968). Aquamarine, for instance, is thought to form at temperatures higher than 300 °C (Andersson, 2019). Yet, some beryl varieties also occur in more restricted constellations (Groat and Turner, 2022). While emeralds may form in pegmatitic or hydrothermal environments, the most well-known deposits occur in shales in Colombia (Karampelas et al., 2019). Furthermore, red beryl forms in rhyolite, and findings have been reported from Utah and New Mexico (Nassau and Wood, 1968; Kimbler and Haynes, 1980; Groat and Turner, 2022). These beryls are believed to have crystallised in two different processes. One set of crystals is found in cavities within rhyolite and is believed to have grown from magmatic vapour. The other beryls, which are present in fractures, are thought to have formed from an approximately 600 °C hydrothermal fluid (Groat and Turner, 2022). As opposed to beryls in pegmatites, which can reach sizes of several centimetres or even metres (Groat and Turner, 2022), red beryls are smaller and often only a few millimetres in size.

2 Materials and methods

The spectra presented here for illustration of the phenomena discussed were obtained on different beryl varieties. The sample set included yellow, green, blue, pink and colourless beryl varieties with different colour saturation. They originated from different localities and geological settings. Apart from one of the emeralds, of which Raman spectra and spectra in the near-infrared (NIR) and mid-infrared (MIR) range are shown, the samples for this study belong to the collection of the German Gemmological Association. The original data (UV–Vis–NIR spectra) of these samples are presented

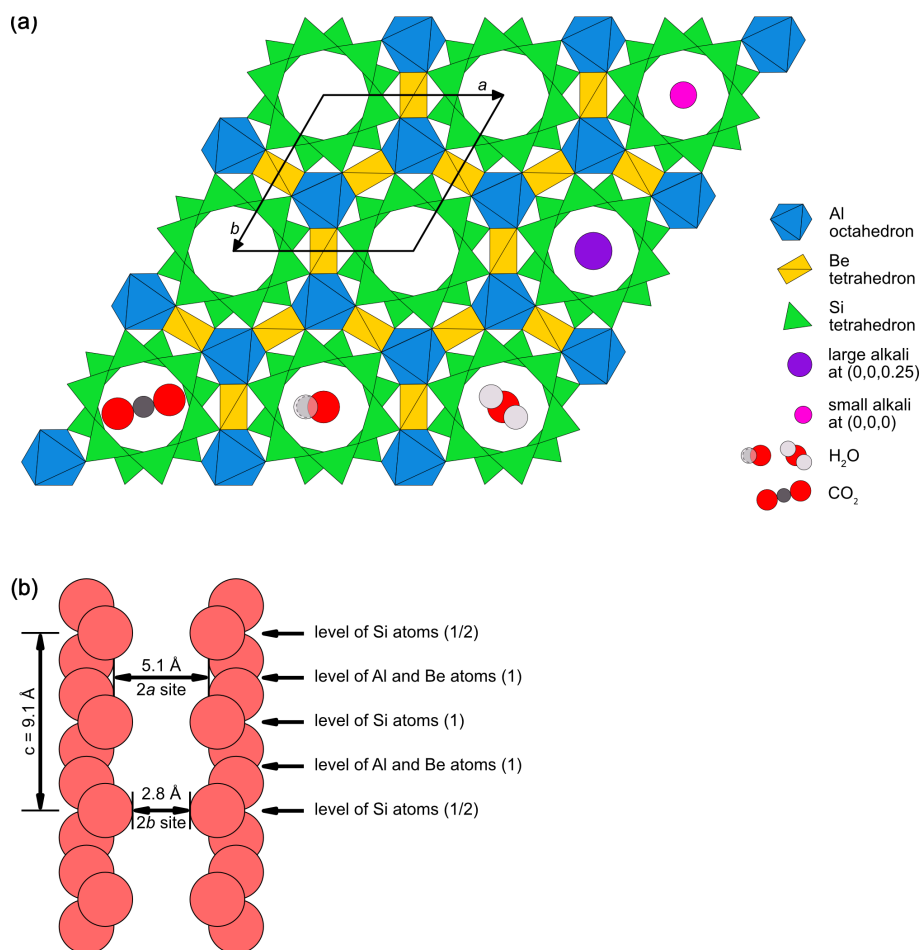


Figure 1. (a) Beryl structure as seen down the c axis of the crystal. Si tetrahedra, Al octahedra and Be tetrahedra are displayed as green, blue and yellow polyhedra. The black rhombus indicates the unit cell edges along the axes a and b . The space between the Si tetrahedra can be filled with various different ions, such as Na (pink circle) or Cs, Rb or K (purple circle), or molecules such as CO₂ (below left) or H₂O in different orientations (below middle and right). (b) The beryl structure as seen perpendicular to the c axis. Successive layers of Si tetrahedra rings seen in panel (a) form channels parallel to the c axis. For a better overview only the channel wall O atoms are depicted in light red. The channels contain cavities of 5.1 Å and bottlenecks of 2.8 Å at which the respective sites 2a and 2b are located. The levels of the Al, Be and Si polyhedral are marked with arrows (diagrams modified after Łodziński et al., 2005; Gatta et al., 2006; McMillan et al., 2006; Groat et al., 2010; Fukuda, 2012; Arivazhagan et al., 2017; Fridrichová et al., 2018; Taran and Vyshnevskiy, 2019; Wang et al., 2021).

to illustrate the typical absorption spectra of the different beryl varieties and facilitate the comparison between them. The other emerald originated from Chitral, Pakistan, and was analysed in more detail in Hanser et al. (2022) (therein referred to as sample PK1). Details on the samples can be found in Table 2. All samples are plane-parallel with the c axes lying in the same plane as the polished faces. Polarised FTIR, Raman and UV–Vis–NIR spectra were acquired as described in Hanser et al. (2022, 2023).

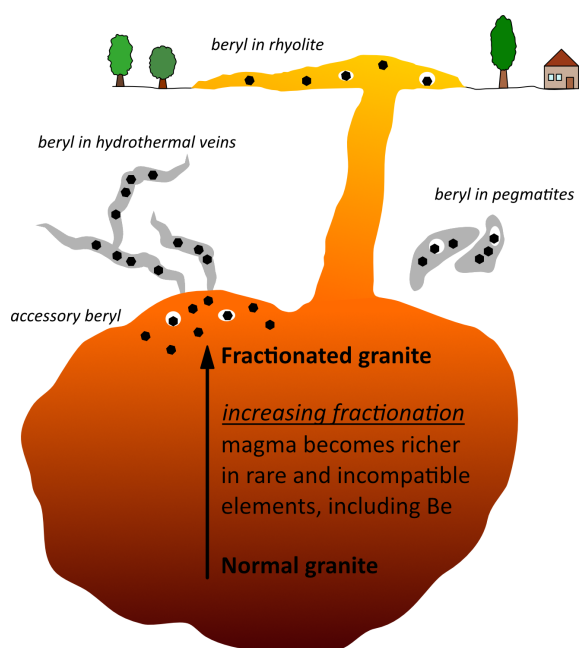
Instrument and measurement details for the different spectra can be found therein. However, only 10 accumulations were acquired for the UV–Vis–NIR spectra of the beryl samples shown in Fig. 3.

3 Colours and varieties of beryl

The chemical formula of beryl does not contain colouring elements. However, there is a range of possible impurities in beryl that can cause colour (Groat and Turner, 2022). The main focus of research lies on the transition metal ions like Fe, Cr, V and Mn which can affect the colour of beryl (Table 1). Nonetheless, the concentration of these metal ions alone is only one of several parameters to play a role in the genesis of colour in a beryl sample. The valence state and the site which is occupied by the elements in question may also influence the colour seen. Since the colour-causing metal ions differ between the beryl varieties, different mechanisms are thought to be responsible for the colour (Nassau, 1978; Mathew et al., 2000). According to a classification pro-

Table 2. Details on the samples of which spectra are presented.

Beryl variety	Colour	Country of origin	Region/mine/locality	Analysis shown	Figure
green beryl	dark green	Nigeria	unknown	UV–Vis–NIR spectrum	Fig. 3
yellow beryl	light yellow	Zambia	unknown	UV–Vis–NIR spectrum	Fig. 3
aquamarine	medium blue	Vietnam	unknown	UV–Vis–NIR spectrum	Fig. 3
emerald	dark green	Türkiye	Eskişehir	UV–Vis–NIR spectrum	Fig. 3
goshenite	colourless	Pakistan	unclear	UV–Vis–NIR spectrum	Fig. 3
morganite	pink	Madagascar	unknown	UV–Vis–NIR spectrum	Fig. 3
emerald	medium green	Pakistan	Chitral region	FTIR spectra (MIR and NIR range) NIR range of UV–Vis–NIR spectrum	Fig. 5 Fig. 7 Fig. 9

**Figure 2.** Schematic representation of magmatic and pegmatitic occurrences of beryl. The black hexagons represent beryl, while the white ellipses around them indicate cavities, in which beryl may form (modified after Groat and Turner, 2022).

posed by Bakakin et al. (1970), “normal”, “tetrahedral” and “octahedral” beryls are recognised with regard to the substituting ion and substitution site (Auriscchio et al., 1988; Andersson, 2006). These different types of beryl can be distinguished spectroscopically in the 1200–400 cm⁻¹ infrared range (Łodziński et al., 2005). In the cases of tetrahedral and octahedral beryls, substitutions primarily occur at the Be and Si tetrahedral sites or at the octahedral site, normally occupied by Al, respectively. In normal beryl, substitutions can occur at these two types of sites simultaneously, yet the extent of each substitution is lower than that in tetrahedral or octahedral beryls with regard to the particular site. Apart

from changes in the IR spectra as a result of these different substitutions, the ratio between the lengths of the crystallographic axes c and a (c/a) has been shown to change alongside and can therefore be used for determining the type of beryl (Auriscchio et al., 1988; Groat et al., 2010). Thus, the changes regarding the axes explain the differing unit cell parameters found by different authors. The most important chromophores (colouring elements) in beryl are Fe, Cr, Mn and V. Yet contrary to other minerals and gemstones, experiments to implant these chromophores into colourless beryl have only led to them entering the channel or interstitial sites and have not resulted in any considerable changes in the colour observed (Mittani et al., 2002a). Though doping and diffusion of these chromophores into beryl were also successful in the later study of Mittani et al. (2004), the position of these transition metal ions could not be determined. It is important to note that beryl samples may contain more than one substituting ion or colour centre and mixed colours may occur. In addition, some types of ions may be able to occupy different sites simultaneously, as is thought to be the case for Fe ions, for instance. Owing to this possibility, many hypotheses have been made with regard to the colour-inducing crystallographic sites and processes involving Fe ions.

3.1 Pink, red and purple colours

These colours are related to Mn impurities (Nassau and Wood, 1968; Wood and Nassau, 1968). Although the characteristic peaks between 480 and 545 nm in the optical spectra of red beryl were attributed to Mn²⁺ and related to the almost identical peaks previously found for pink beryl (Nassau and Wood, 1968), Andersson (2013) suggests the colour of morganite (pink to orange-pink) is caused by both Mn²⁺ and Mn³⁺, while Mn³⁺ is proposed to be the sole cause of the colour in red beryl. This argumentation is supported by other authors (Fridrichová et al., 2018). However, in a synthetic purple beryl no changes in optical absorption were induced by annealing. Therefore, the authors concluded that the pur-

ple colour was caused by Mn independent of its valence state (Gaite et al., 2001).

3.2 Blue to yellow colours

The colours of blue beryl and yellow beryl are both attributed to Fe. There are also mixed colours, leading to greenish beryls. However, Fe can be detected in all of the different beryl varieties, with pink beryls (morganites) typically exhibiting low contents (Hu and Lu, 2020). While beryls with other colours usually contain approximately 1 wt % of Fe, the yellow and blue varieties commonly have Fe contents of up to 3 wt % (Fridrichová et al., 2015), with some samples from different localities exceeding this value by about the same amount (Groat et al., 2010). The role of Fe ions in the cause of colours of blue and yellow beryl has largely been studied by heating and irradiation treatments. A yellow beryl can be heated and turned into a blue aquamarine. This practice is commonly applied in the jewellery and gemstone trade and influences the market value the stone has (Blak et al., 1982; Alkmim et al., 2017). It is rooted in the reduction of Fe³⁺ to Fe²⁺ ions (Blak et al., 1982; Alkmim et al., 2017). Though this procedure yields a more desirable blue colour (Chankhantha et al., 2016), it can be reversed by irradiation with high energy, such as γ -rays (Alkmim et al., 2017). This does not only hold true for the colour, but also for the spectral changes induced by heat treatment, which have been observed to be restored by irradiation (Goldman et al., 1978).

Still, there is debate on the precise reason for the blue and yellow colours in beryl as some studies assume the colours are caused by single Fe ions, whereas others consider more complex substitutions and interactions to be responsible. Some authors relate the intensity and the hue of the blue of aquamarine to the concentration of Fe³⁺ and its relative proportion to Fe²⁺ present in the structure (Viana et al., 2002b, a; Skvortsova et al., 2015; Hu and Lu, 2020). Especially with regard to their possible valence states, Fe ions have been suggested to be able to replace Al³⁺ and Be²⁺. Nonetheless, the substitution of Al by Fe ions of either valence state and the substitution of Be by ferrous Fe are regarded not to cause colour in some studies (Andersson, 2019). Some authors have also proposed for Fe to substitute for Si in addition to Al and Be (Viana et al., 2002a; Andersson, 2019), yet again without inducing colour (Andersson, 2019). However, with an ionic radius of about 0.74 Å, Fe²⁺ is more than twice the size of Be²⁺, having an ionic radius of only 0.35 Å (Viana et al., 2002a). The coordination to four O atoms does not change the size difference of Be²⁺ (0.27 Å) compared to Fe²⁺ (0.63 Å) and Fe³⁺ (0.49 Å), respectively (Shannon, 1976; Andersson, 2019). Similarly, the Fe²⁺ ion has more than 1.5× the dimensions of Si⁴⁺, with its ionic radius being only 0.42 Å (Viana et al., 2002a) and 0.26 Å in fourfold coordination with O atoms (Shannon, 1976; Andersson, 2019). Generally, aquamarine of bluish hues have been found to exhibit comparably high amounts

of Fe²⁺ but only little to negligible Fe³⁺ contents. The predominately ferrous valence state of Fe in beryl is also supported by X-ray absorption spectroscopy studies (Figueiredo et al., 2008). With increasing Fe³⁺ or decreasing Fe²⁺ contents, these aquamarines become more greenish as a result of the increasing influence of the yellow colour component from Fe³⁺ ions (Viana et al., 2002b; Pøikryl et al., 2014; Alkmim et al., 2017). If these Fe ions were to occur at the same position within the crystal structure, the lower charge of ferrous Fe in blue aquamarine could explain the higher concentration of type II H₂O (H₂O coordinated with alkalis; for more details see section on alkalis and section on H₂O) in these specimens compared to those of green beryls with their higher relative ferric Fe contents. Since type II H₂O correlates with the amount of alkali ions present in the structural channels counteracting charge imbalance from the substitution of structural components by lower-valence ions (Wood and Nassau, 1967; Viana et al., 2002b; Huong et al., 2010; Alkmim et al., 2017), a higher concentration of Fe³⁺ should require smaller amounts of alkalis for charge compensation and in turn lead to a lower concentration of type II H₂O. This assumption is supported by a study by Fridrichová et al. (2015), in which blue beryls exhibited higher alkali contents than yellow beryls, and findings of Viana et al. (2002b) and Alkmim et al. (2017), who found higher contents of type II H₂O in blue compared to greenish beryl. However, this is the opposite of and thus seems to contradict with what Blak et al. (1982) observed in their study. However, since constituting cations such as Be²⁺ can be missing in some of their structural positions without having been substituted (Wood and Nassau, 1968), a larger need for charge compensation by alkalis can arise and thus increase the type II H₂O content even in green beryl as observed by Blak et al. (1982). Still, it is not possible to say if the beryls in these three studies had different ratios of vacancies within the structure since no crystallographic experiments were performed. Furthermore, substitutions with non-colour-causing ions, such as Mg²⁺, can also increase the lack of positive charges compensated for by alkalis and, consequently, the amount of type II H₂O.

Similar to the effect of the two valence states of Fe ions, the site occupancy and the subsequent possible interactions and subsequent influence on colour between them are unclear or disputed. The Mössbauer studies on blue and greenish aquamarines by Viana et al. (2002a) revealed symmetrical split doublets, the hyperfine parameters of which were similar at 500 K, leading the authors to conclude that their samples contained two or more different Fe²⁺ ion species in sites with similar symmetries. These findings are consistent with previous analyses by Blak et al. (1982), who found the spectra of their green beryls exhibit two distinguished Fe³⁺ species that were subsequently reduced to two different Fe²⁺ species upon heating to obtain the blue aquamarine. Viana et al. (2002a) further observed a small change in quadrupole splitting of their Mössbauer spectra on blue to greenish blue aquamarines with different temperatures, indi-

cating that the sites occupied by Fe ions were distorted. Similar to Nassau (1994), Viana et al. (2002a) assigned Fe²⁺ to the channels, causing a blue colour, and Fe³⁺ to the Al³⁺ octahedral site, resulting in a yellow colour. In contrast to this, trivalent Fe has been suggested to not induce colour in beryl (Andersson, 2019). Moreover, further authors assume inter-valence charge transfer (IVCT) to play a role in the colour of aquamarine (Nassau, 1978; Mathew et al., 2000), presumably taking place between Fe²⁺ and Fe³⁺ ions (Fridrichová et al., 2015; Andersson, 2019). Mathew et al. (2000) explained the colour change of an irradiated yellow beryl sample to blue during heating by an increase in Fe²⁺ and IVCT between adjacent Fe²⁺ and Fe³⁺ ions, which can be located at multiple sites. However, K-edge X-ray spectra using synchrotron radiation revealed the 6g interstitial site next to the Al site, which is located at (1/3, 2/3, 1/2) and had already previously been suggested to be a site for substitutions by Fe (Goldman et al., 1978; Groat et al., 2010), as well as the octahedral Al site itself to be occupied with Fe ions (Lin et al., 2013). Both sites have thus been proposed as the two possible adjacent locations for the Fe²⁺ and Fe³⁺ ions engaging in IVCT (Lin et al., 2013). Nevertheless, IVCT remains questionable in some cases according to other authors (Pøikryl et al., 2014). Furthermore, Andersson (2019) proposed two different IVCT mechanisms for light blue aquamarine and darker blue beryls. Another study also indicated that the presence of Fe in both valence states at octahedral and interstitial sites may be the reason for a darker blue colour in some samples (Bunnag et al., 2020). Similar to aquamarine, the colour of yellow beryl has not only been attributed to Fe³⁺ alone, but also to a charge transfer involving Fe³⁺ and O²⁻, with an associated absorption extending from the blue to the UV part of the spectrum. This is, therefore, also referred to as ultraviolet charge transfer, UVCT (Fritsch and Rossman, 1988). However, in more recent studies, yellow beryls are further subdivided into heliodor and golden beryl on the basis of differing spectral features (Platonov et al., 2016; Andersson, 2019; Shang et al., 2022). Both shades of yellow colour are attributed to Fe³⁺, yet with the ions supposedly occupying different sites. According to this classification, they substitute for Al in its octahedral position in heliodor, whereas in golden beryl the substitution takes place in the Be tetrahedron (Andersson, 2019; Shang et al., 2022). Moreover, Andersson (2019) suggests that heliodor does not contain sufficient amounts of ferric ion pairs that could result in IVCT and turn these yellow beryls into blue aquamarines upon heating. The author argues that heliodors simply lose their colour during heating, while the only yellow beryls to turn blue would be termed golden beryls (Andersson, 2019). However, many studies do not distinguish between both yellow hues, and the terms may sometimes be used interchangeably for yellow beryls, thus making comparisons of data difficult. The same is true for blue colours of various intensities, which are usually referred to as either aquamarine or blue beryl, with no further distinction being made.

In addition to these differing conclusions on the colour mechanisms involving Fe ions, the possibility for Fe²⁺ and Fe³⁺ to be incorporated into the channels of beryl is equally unclear. While Fe ions could theoretically be present in all three types of sites (tetrahedral, octahedral, channel) within beryl (Fridrichová et al., 2015), some authors argue that especially ferrous Fe ions are too large to replace Al directly and thus may enter the channel instead, which could provide more space for Fe²⁺ (Bunnag et al., 2020). Fe³⁺ has more recently also been proposed to occupy the channels and form Fe hydrate [Fe₂³⁺(OH)₄]²⁺ with the H₂O molecules there (Yu et al., 2017; Wang et al., 2022a). The resulting hydrate was suggested to induce a yellow colour (Wang et al., 2022a). Although several authors including, for instance, Wood and Nassau (1967), Goldman et al. (1978) and Blak et al. (1982) also attributed some optical features observed in beryl to Fe ions located in the channels, other studies have found only little Fe in the channel site, in spite of a high general Fe content (Groat et al., 2010). Similarly, Andersson (2013) found no evidence to support the interpretation of previous studies on the presence of Fe ions in the channels of beryl. Likewise, investigations on synthetic beryls showed no Fe in the channels (Adamo et al., 2008b). Yet, a recent atomic resolution image taken with a transmission electron microscope on a heliodor from Vietnam revealed the channels to be occupied with ions (Arivazhagan et al., 2017). The lower atomic numbers, scattering powers and amounts of other trace elements led the authors to conclude that Fe was the only trace element of suitable concentration with a high enough atomic number and subsequently sufficient scattering power to show in the image. However, as a result of beam damage, a low critical dose was applied, which made further supplementary spectroscopic analyses impossible (Arivazhagan et al., 2017). Thus, the presence of ferrous and ferric Fe in the channels of beryl remains disputed.

Problems do not only arise from the possibility of Fe²⁺ and Fe³⁺ being able to theoretically occupy multiple sites in the structure of beryls (Pøikryl et al., 2014; Fridrichová et al., 2015), but also from the detection of the different valence states of Fe by various analytical methods. For instance, while Fe³⁺ can easily be analysed with electron paramagnetic resonance (EPR) at room temperature, the detection of Fe²⁺ requires low temperatures (Andersson, 2013) down to the temperature of liquid helium or 4 K as a result of the small spin relaxation time of divalent Fe (Mathew et al., 2000). In addition, owing to the possible substitutions of the constituting elements of beryl, the chemical composition of beryl is variable (McManus et al., 2008; McMillan et al., 2006), thus resulting in difficulties when looking for elements suitable as internal standard for analyses such as LIBS (McMillan et al., 2006).

While the blue colour of aquamarine is stable, there are beryl varieties which lose their blue hues when subjected to light (Nassau and Wood, 1973; Nassau et al., 1976; Adamo et al., 2008a). This may also happen under the influence of heat

(Adamo et al., 2008a). In contrast to aquamarine, these beryl varieties do not owe their colours to Fe, which was shown to be below detection limit in these samples, but to different colour centres (Adamo et al., 2008a). The intense blue Maxixe beryls are natural beryls, the colour of which is attributed to free NO₃ radicals having formed as a result of natural radiation and which are located within the hexagonal channels. The colour of Maxixe-type beryls is caused by free radicals of CO₃⁻ also located in the channels (Nassau et al., 1976; Edgar and Vance, 1977; Andersson, 1979; Mathew et al., 2000; Krambrock et al., 2002; Mittani et al., 2002b; Andersson, 2008, 2010, 2019; Skvortsova et al., 2015). These colour centres can, however, also be induced by artificial irradiation, for instance, using neutrons (Edgar and Vance, 1977; Mathew et al., 2000; Skvortsova et al., 2015). Exposure to light causes NO₃ and CO₃⁻ to turn into NO₃[•] and CO₃^{2•-}, leading to the subsequent loss of colour (Andersson, 2008).

3.3 Green colours

The green colour of emerald is caused by three-valent Cr ions, and the colouring mechanism is explained by the crystal field model (Nassau, 1978; Burns, 1993). The Al octahedron is the site occupied by Cr³⁺ (Wood and Nassau, 1968; Groat and Turner, 2022). However, the green colour can also be caused or influenced by V (Schwarz et al., 1996; Stephan et al., 2019; Krzemnicki et al., 2020). This possibility has caused debate about whether the variety term emerald should be reserved for Cr-coloured beryl of sufficient colour saturation only (Hänni, 1992; Schwarz et al., 1996).

In addition to the green colour of emerald, green colour in beryl can also be the result of a mixture of yellow- and blue-colouring mechanisms and can thus also be related to Fe impurities (Blak et al., 1982; Mathew et al., 2000; Skvortsova et al., 2015). Nonetheless, since the exact positions of the Fe ions causing yellow and blue colours remain under debate in yellow and blue beryls, so do their locations in Fe-coloured green beryl. Fe may also influence the green colour of emerald (Hänni, 1992; Krzemnicki et al., 2020, 2021).

3.4 Colourless

With regard to the impurities and effects of the coloured varieties, colourless beryl (goshenite) is sometimes described as “pure” as the chemical formula of beryl does not contain colour-inducing elements. Still, goshenite can contain impurities. In contrast to the varieties listed above, a number of reasons may apply as to why these impurities do not cause colouration. The absorption bands may lie too far in the NIR or UV region and not be strong enough to affect the colour seen (Lind and Stephan, 2022). The impurities may not be able to induce colouration (as in the case of Mg), they may be located in a non-colour-causing site or they may be present in a valence state not suitable to affect the colour, as for example tetravalent Ti (Nassau and Wood, 1968). This assump-

tion is supported by experiments in which colourless beryl displayed a change in colour to yellow and blue upon irradiation and heating. The related Mössbauer spectra showed colourless beryl contained Fe³⁺ ions (Mathew et al., 2000). While Mathew et al. (2000) assigned this Fe³⁺ to a position within the channel of beryl, Andersson (2013, 2019) argues for this Fe³⁺ to be able to occupy the octahedral Al³⁺ position on the assumption that this would be a non-colour-causing site for Fe³⁺, consistent with the work of previous authors (Mihalynuk and Lett, 2003). Likewise, the occupation of the tetrahedral site by Fe²⁺ was regarded to not cause colour in beryl (Andersson, 2019). However, these suggestions contradict previous works which explained the yellow colour of heliodor by ferric Fe in the octahedral site, whereas ferrous Fe in the same site was reported to not induce colour in beryl (Nassau, 1994; Viana et al., 2002a; Fridrichová et al., 2015).

Table 3 lists a selection of spectral absorptions of beryl found in the literature and the cause they have been related to during the last decades. As can be seen, absorption bands at similar or identical positions are attributed to ions at different possible sites or to different causes entirely. In some cases, however, the possible causes remain unclear. Examples of typical UV–Vis–NIR spectra of beryls of different colours are shown in Fig. 3. The spectra are polarised so that the electric field vector *E* of the incident light is perpendicular to the *c* axis of the sample (*E*⊥*c*) in one direction and parallel (*E*∥*c*) in the other. It can be seen that absorption commonly attributed to Fe can be distinguished in the direction *E*⊥*c* in all but pink morganite samples. This also includes the apparently pure colourless beryl variety goshenite. Furthermore, emerald spectra exhibit two broad bands in both directions (*E*⊥*c* and *E*∥*c*), which are not commonly found in other beryl varieties and have thus been related to Cr and/or V. The presence of a pronounced Fe-related absorption at around 830 nm in NIR, compared to the Cr and V absorptions in the visible region, can help in determining the geographic origin for gem quality emeralds. It is usually prominent in schist-hosted emeralds, whereas emeralds from localities like Colombia and the Panjshir Valley, Afghanistan, only show minor or no Fe-related absorption in this region of the spectrum (Karampelas et al., 2019; Saeseaw et al., 2019; Krzemnicki et al., 2021; Hanser et al., 2022, 2023). Yet, the figure also illustrates that while other green beryls (those which are neither coloured by Cr nor V) lack these Cr and V absorption bands entirely, their spectra represent a mixture of the spectral features seen in aquamarine and yellow beryl. According to earlier works, all of the yellow beryls presented here would be termed heliodor instead of golden beryl, as there is a strong Fe²⁺ absorption visible in the *E*⊥*c* direction (Andersson, 2019; Shang et al., 2022). Furthermore, contrary to what was reported by Andersson (2019), no significant differences could be observed in the light blue and dark blue beryl spectra analysed.

Table 3. Selection of absorptions in UV–Vis–NIR found in beryl of different colours and the possible cause and/or site they have been attributed to.

Absorption/ signal [nm]	Approximate absorption/ signal [cm ⁻¹]	Polarisation	Analysis	Colour of beryl	Cause/site	Reference
372 nm	26 882	not mentioned	optical absorption		Fe ³⁺	Goldman et al. (1978)
372.5 nm	26 846	E⊥c	optical absorption	green	Fe ³⁺	Gübelin (1989)
375 nm	26 667	not mentioned	optical absorption	blue	Fe ³⁺	Fridrichová et al. (2015)
400 nm (tail extending to UV light)	25 000	not mentioned	optical absorption	yellow	Fe ³⁺ at Al ³⁺	Mathew et al. (2000); Mittani et al. (2002a)
400 nm absorp- tion edge	25 000	not mentioned	optical absorption	yellow	not mentioned	Fridrichová et al. (2015)
420 nm (band)	23 810	E⊥c	optical absorption	green	Fe ³⁺	Gübelin (1989)
425 nm	23 529	not mentioned	optical absorption		not mentioned	Goldman et al. (1978)
425 nm	23 529	not mentioned	optical absorption	blue	Fe ³⁺	Fridrichová et al. (2015)
430 nm (band)	23 256	E⊥c	optical absorption	green	Fe ³⁺	Gübelin (1989)
430 nm (band)	23 256	not mentioned	optical absorption	green	Cr ³⁺ at Al ³⁺	Wood and Nassau (1968)
430 nm (band)	23 256	not mentioned	optical absorption	green	Cr ion electronic transitions	Skvortsova et al. (2015)
445 nm	22 472	E⊥c	optical absorption	green	Fe ³⁺	Gübelin (1989)
476 nm	21 008	not mentioned	optical absorption	green	Cr ³⁺ at Al ³⁺	Wood and Nassau (1968)
477.4 nm	20 947	E⊥c	optical absorption	green	Fe ³⁺	Gübelin (1989)
540 nm (band)	18 519	σ	optical absorption	red	Mn ³⁺	Andersson (2013)
560 nm (band)	17 857	π	optical absorption	red	Mn ³⁺	Andersson (2013)
600 nm (band)	16 667	not mentioned	optical absorption	green	Cr ³⁺ at Al ³⁺	Wood and Nassau (1968)
604 nm	16 556	E⊥c	optical absorption	green	Cr ³⁺	Gübelin (1989)
620 nm	16 129	E∥c	optical absorption		Fe ²⁺ in channel	Wood and Nassau (1968)
620 nm	16 129	E∥c	optical absorption		Intervalence charge transfer Fe ²⁺ /Fe ³⁺	Parkin et al. (1977)
630 nm	15 873	E∥c	optical absorption	green	Cr ³⁺	Gübelin (1989)
637 nm	15 699	E⊥c	optical absorption	green	Cr ³⁺	Gübelin (1989)
646 nm	15 480	E∥c	optical absorption	green	Cr ³⁺	Gübelin (1989)
662 nm	15 106	E∥c	optical absorption	green	Cr ³⁺	Gübelin (1989)
680 nm	14 706	E∥c	optical absorption	green	Cr ³⁺ at Al ³⁺	Wood and Nassau (1968)

Table 3. Continued.

Absorption/ signal [nm]	Approximate absorption/ signal [cm ⁻¹]	Polarisation	Analysis	Colour of beryl	Cause/site	Reference
680 nm	14 706	E⊥c	optical absorption	green	Cr ³⁺	Gübelin (1989)
683 nm	14 641	E∥c	optical absorption	green	Cr ³⁺ at Al ³⁺	Wood and Nassau (1968)
685 nm	14 599	E⊥c	optical absorption	green	Cr ³⁺	Gübelin (1989)
740 nm	13 514	not mentioned	photoluminescence	various	Fe ²⁺	Skvortsova et al. (2015)
810 nm	12 346	E⊥c	optical absorption		Fe at Al ³⁺	Wood and Nassau (1968)
810 nm	12 346	E⊥c	optical absorption		Fe ²⁺ at Al ³⁺	Parkin et al. (1977)
810 nm	12 346	E⊥c	optical absorption		Fe ²⁺ at tetrahedral site	Price et al. (1976)
810 nm	12 346	E∥c	optical absorption		Fe ²⁺ in channel site	Goldman et al. (1978)
810 nm	12 346	E∥c	optical absorption		Fe in channel	Wood and Nassau (1968)
810 nm	12 346	E∥c	optical absorption		Fe ²⁺ at Al ³⁺	Price et al. (1976)
810 nm	12 346	not mentioned	optical absorption	blue	Fe ²⁺	Fridrichová et al. (2015)
813 nm	12 300	not mentioned	optical absorption	green	electron transitions of Fe ²⁺ at Al site	Skvortsova et al. (2015)
1000 nm	10 000	E∥c	optical absorption		Fe in channel	Wood and Nassau (1968)
1000 nm	10 000	E∥c	optical absorption		Fe ²⁺ at Al ³⁺	Price et al. (1976)

* E⊥c: electric field vector of incoming light perpendicular to *c* axis; E∥c: electric field vector of incoming light parallel to *c* axis; σ: perpendicular to *c* axis; π: parallel to *c* axis.

4 Channel occupancy by alkalis, H₂O and CO₂

Since beryl exhibits structural channels formed by the stacked Si tetrahedra rings (Fig. 1), the uptake of non-framework ions and molecules is possible. A variety of different species can be located in the structural channels depending on the type of beryl and/or its genesis. Thus, synthetic beryls have been reported to contain ammonium (Mashkovtsev and Solntsev, 2002), while the colours of Maxixe and Maxixe-type beryl have been attributed to channel NO₃⁻ and CO₃²⁻, having formed from NO₃⁻ and CO₃²⁻ by natural or artificial radiation, respectively (Mathew et al., 2000; Krambrock et al., 2002; Andersson, 2013). However, the most common species found in the channels of beryl are H₂O molecules, alkali ions and CO₂ molecules. Therefore, this paper will focus on these only.

4.1 Alkalis

Since the substitutions in beryl can take place with lower-valence ions than its original components, a lack of positive charges arises (Aurisicchio et al., 1988; Fridrichová et al., 2018; Andersson, 2019). It has been proposed that alkali metal ions compensate for charge deficiencies resulting from substitution of Al, Si and Be by transition metal ions of lower valence state by entering the channels of beryl (Wood and Nassau, 1968; Aurisicchio et al., 1988; Fukuda, 2012; Fridrichová et al., 2018). Although alkali ions and H₂O have previously been proposed to occupy the aforementioned 2*a* and 2*b* positions, respectively (Fig. 1) (Aurisicchio et al., 1988), the majority of studies suggest smaller ions are located at the 2*b* site, whereas H₂O molecules and larger ions, including Cs, are located at the 2*a* site within the channels of beryl (Hawthorne and Černý, 1977; Andersson, 2006; Gatta et al., 2006; Hu and Lu, 2020).

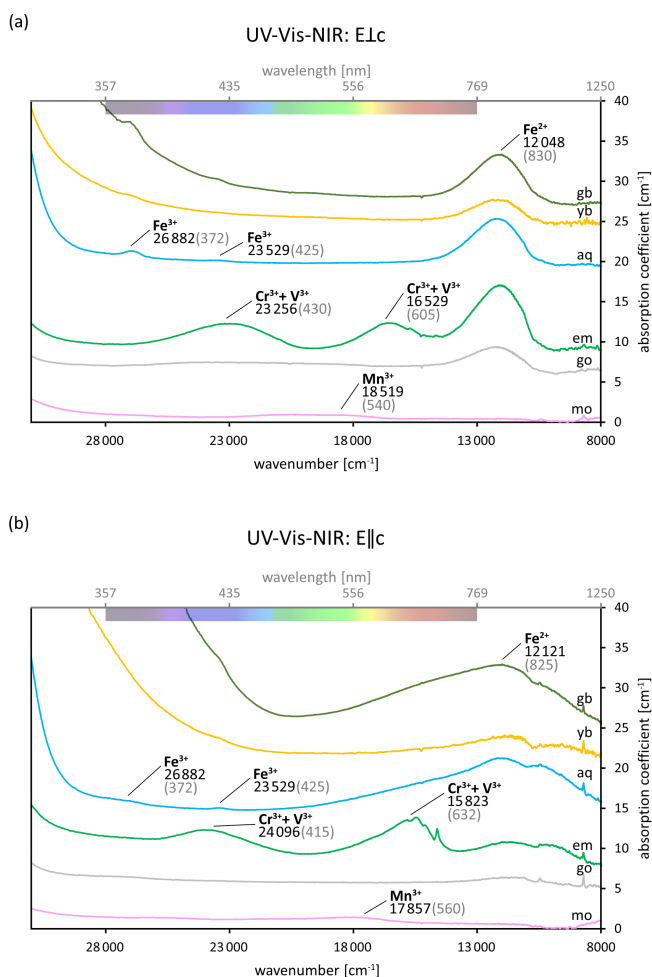


Figure 3. (a–b) UV–Vis–NIR spectra of differently coloured beryl varieties (mo: morganite; go: goshenite; em: emerald; aq: aquamarine; yb: yellow beryl; gb: green beryl) in E \perp c (a) and E \parallel c (b) directions illustrating the absorptions discussed in the “Colours and varieties of beryl” section. The supposed causes of the absorptions are labelled with their approximate positions given in wavenumbers (black) and corresponding wavelengths (in grey parentheses). Some of the positions slightly differ from those reported in the literature (see Table 3). The coloured bar at the top shows the approximate colours of the visible part of the spectrum. Fe-related absorption is visible in almost all spectra. Contrary to this, Cr- and V-related absorption can be observed in the emerald spectra only. The graphs have been offset for clarity.

Several authors have shown that Li may enter the *2b* channel site (Sherriff et al., 1991; Andersson, 2006; Adamo et al., 2008b). However, a dependence of the Li content and the length of the unit cell edge *c*, which has been found to increase with an increasing amount of Li and Be vacancies in the samples, has been demonstrated, whereas the length of the unit cell edge *a* was shown not to be as affected (Bakakin et al., 1970). It was thus assumed that Li replaces Be directly in the Be tetrahedra (Aurisicchio et al., 1988; de Almeida Sampaio Filho et al., 1973; Hawthorne and Černý, 1977),

thus also affecting the bond lengths within the crystal structure as a result of the bond strength deficiency induced by the substitution (Hawthorne and Černý, 1977). An alternative explanation in which Li is, in fact, still located at a tetrahedral site but an interstitial one adjacent to the actual Be²⁺ tetrahedron instead has also been suggested (Andersson, 2006, 2013, 2019). In spite of previous studies on isomorphic substitutions of Be²⁺ by Co³⁺ and Cu²⁺ (Solntsev et al., 2004) and the similar radii of these ions compared with Li⁺, Andersson (2006, 2013, 2019) argues for Li to occupy the aforementioned interstitial site. This distorted tetrahedron is supposed to span between one face of the Be tetrahedron and one of the nearest O atoms in the Si tetrahedra rings. Moreover, owing to the structural arrangement in beryl, each of the four Be tetrahedra faces creates an equivalently distorted tetrahedron with its nearest O atoms (Andersson, 2006, 2019). Another interstitial site has also been discussed in these studies as a possible location of Li in beryl. Notwithstanding, the close proximity of positively charged Si and the inaccessibility of the site via the channel is thought to make it a less probable site than the distorted tetrahedron (Andersson, 2006). While Li might substitute for Be, it is unlikely to substitute for Al as this would be an unfavourable substitution because of bond strength deficiency (Aurisicchio et al., 1988). This assumption is supported by previous studies which found no Li at the octahedral Al site (Hawthorne and Černý, 1977).

In contrast to Li, the exact location of which remains disputed in the literature, it is generally agreed that Na⁺ enters the beryl channels where it is coordinated with H₂O molecules (see next section). Most studies find Na to occupy the *2b* site (Hawthorne and Černý, 1977). However, this might only apply to hydrous beryl, whereas in beryls with low or no H₂O content, it could also be located at the *2a* site, which is normally thought to be occupied by H₂O (Artioli et al., 1995). Besides Na possibly being able to occupy both sites, *2a* and *2b*, when alone (Andersson, 2006), the dimensions of the channel at the *2a* site could also allow Na and H₂O to occupy it simultaneously (Alkmim et al., 2017). Similar to Na, cations such as K⁺ and Cs⁺ are also present in the channels. However, because of their large sizes, they have been assigned to the *2a* site (e.g. Hawthorne and Černý, 1977; Viana et al., 2002a; Gatta et al., 2006). Similar to Li, Na is thought to narrow the dimensions of the channel site it is located in (Andersson, 2006). Contrary to earlier studies, which reported channel impurities to not affect beryl’s unit cell parameters (Blak et al., 1982), leaching experiments have found the release of alkali ions to induce a decrease thereof (Manier-Glavinaz et al., 1989).

4.2 H₂O

The large channels within the beryl crystal structure allow the diffusion of H₂O through them (Fukuda et al., 2009). Thus, H₂O is often found in beryl, though beryl is, by definition, an anhydrous mineral. So far, only red beryl from Utah

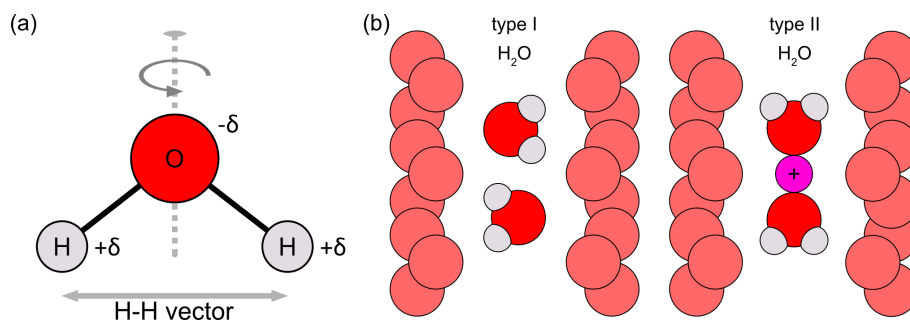


Figure 4. (a) H₂O molecule showing the twofold symmetry axis (dashed line) and the H–H vector between both hydrogen atoms. The H₂O molecule is partially charged. These charges are denoted as $+\delta$ for the positive charges (at H atoms) and $-\delta$ for the negative charge (at O atom). (b) Structural channels of beryl showing the type I H₂O (left) and the type II H₂O (right) configurations. The channel O atoms are displayed in light red. Small channel alkali cations, such as Na, causing the orientation change of type I to type II H₂O, are shown in pink (modified after Łodziński et al., 2005; Fukuda and Shinoda, 2008; Fukuda, 2012; Belyanchikov et al., 2017; Wang et al., 2021).

has been shown not to contain any H₂O (Nassau and Wood, 1968; Aurisicchio et al., 1988; Andersson, 2013). This can also be used to differentiate between natural red beryls and their synthetic counterparts (Gatta et al., 2022). Aurisicchio et al. (1988) proposed that H₂O molecules could act to fill the gaps caused by the structural channels and establish a closest packing of the O layers with the H-bond lengths of the H₂O molecules being equivalent to the distance of the channel O atoms from the centre of the channel.

The presence of H₂O in beryl has largely been studied with the help of (FT)IR spectroscopy. According to Krambrock et al. (2002), the infrared spectra of beryl can be divided into three different ranges. The lower wavenumbers, ranging from 400 to 1250 cm⁻¹, are attributed to the general constituting chemical components of beryl, BeO₄, AlO₆, and SiO₄ and their vibrational modes (Krambrock et al., 2002; Łodziński et al., 2005), whereas the higher wavenumber ranges reveal whether additional molecules and H₂O are present (Krambrock et al., 2002; Wood and Nassau, 1968). Apart from some bands becoming sharper during cooling, as a result of the hindered thermal motions, the IR spectrum of beryls in the region between 400–1300 cm⁻¹ remains unchanged in different beryl samples during heating and cooling experiments according to Łodziński et al. (2005).

In the case of H₂O molecules, three vibrational modes are distinguished: ν_1 , ν_2 and ν_3 . Aurisicchio et al. (1988) suggested H₂O molecules to be able to occupy both the 2a and 2b positions in some beryl samples, thus giving rise to two different peaks in the IR spectra of beryl. Another explanation for these two differing peaks, based on the orientation of the H₂O molecules within the channel, is generally accepted. An H₂O molecule can be orientated in two ways within the beryl channel (Fig. 4). In the first case, when the twofold symmetry axis of the H₂O molecule is perpendicular to the *c* axis of the beryl crystal, the orientation is referred to as type I H₂O (e.g. Aines and Rossman 1984; Bidny et al., 2011; Mashkovtsev et al., 2016). As can be seen from Fig. 4,

the H–H vector is thus parallel to the channel length (e.g. Wood and Nassau, 1967; Aines and Rossman, 1984; Kolesov and Geiger, 2000; Viana et al., 2002b; Fukuda and Shinoda, 2008). More detailed structural studies suggest that the orientation is, in fact, only quasi-parallel with a slight inclination of approximately 4° of the H–H vector from the *c* axis (Gatta et al., 2006). The other type of H₂O in beryl is type II H₂O, for which the twofold axis of the molecule is parallel to the beryl channel and with the H–H vector thus being perpendicular to it (e.g. Wood and Nassau, 1967; Kolesov and Geiger, 2000; Viana et al., 2002b; Fukuda and Shinoda, 2008; Bidny et al., 2011). Furthermore, the difference in orientation causes differences in the vibration modes of H₂O and the peaks observed at specific frequencies (Table 4).

The dipole moment of the H₂O molecule would enable interactions via H bonding between the H₂O molecule in the channel and the O atoms of the channel walls. While such electrostatic interactions would be expected to influence the vibrational modes and no such frequency shifts had previously been observed in the IR spectra of beryl (Wood and Nassau, 1968), a change in the vibrational frequencies of Raman spectra was shown to occur while cooling beryl (Kolesov, 2008). However, other authors regard the channel dimension to be inappropriate to allow for H bonding with the H₂O molecules within to occur (Gatta et al., 2006). Furthermore, site population analyses with the help of neutron diffraction found only weak H bonding (Artioli et al., 1993). An alternative explanation of a long-range interaction of the beryl structure with the H₂O molecules has thus been proposed (Kolesov and Geiger, 2000; Gatta et al., 2006). Regardless of the nature of the interaction, type I H₂O is the main type of H₂O present in pure, unsubstituted beryl, also referred to as normal beryl (Fukuda and Shinoda, 2008; Charoy et al., 1996), and forms the most important impurity in beryl in general (Wood and Nassau, 1967). However, beryl can also contain alkalis, especially Na⁺, in its channels. This uptake is thought to be rooted in the compensation of charge

Table 4. Fundamental IR-active vibrational modes of H₂O in beryl.

Molecule	Type	Coordination	Vibrational mode	Type of vibration	Wavenumber [cm ⁻¹]	Polarisation	
H ₂ O	I	uncoordinated	ν_1	symmetric stretching (Aines and Rossman, 1984; Viana et al., 2002b)	3555 (Aines and Rossman, 1984; Mashkovtsev and Lebedev, 1993; Viana et al., 2002b; Wood and Nassau, 1968; Bidny et al., 2011; Wood and Nassau, 1967)	E _{1c} (Charoy et al., 1996; Fukuda, 2012; Aines and Rossman, 1984; Wood and Nassau, 1967)	
					3605 (Fukuda, 2012)		
					3647/3630/3610 (Łodziński et al., 2005)		
H ₂ O	I	uncoordinated	ν_2	bending (Charoy et al., 1996; Aines and Rossman, 1984)	1542 (Wood and Nassau, 1968; Bidny et al., 2011)	E _{1c} (Charoy et al., 1996; Fukuda, 2012; Aines and Rossman, 1984; Wood and Nassau, 1967)	
					1594 (Mashkovtsev and Lebedev, 1993)		
					1595 (Aines and Rossman, 1984; Wood and Nassau, 1967)		
					triplet (1640, 1600, 1546) (Fukuda, 2012)		
					1602/1550 (Łodziński et al., 2005)		
H ₂ O	I	uncoordinated	ν_3	asymmetric stretching (Aines and Rossman, 1984; Viana et al., 2002b)	3694 (Mashkovtsev and Lebedev, 1993; Viana et al., 2002b; Wood and Nassau, 1968; Bidny et al., 2011)	E _{1c} (Charoy et al., 1996; Fukuda, 2012)	
					3698 (Fukuda, 2012)		
					triplet (3521, 3694, 3860) (Wood and Nassau, 1967)		
					3697/3690 (Łodziński et al., 2005)	triplet (E _{1c} , E _{1c} , E _{1c}) (Wood and Nassau, 1967)	
II	single Na ⁺ -H ₂ O (Mashkovtsev et al., 2016; Fukuda and Shinoda, 2008; Fukuda, 2012)		ν_1	symmetric stretching (Viana et al., 2002b)	3589 (Mashkovtsev et al., 2016; Fukuda and Shinoda, 2008; Fukuda et al., 2009)	E _{1c} (Charoy et al., 1996)	
					3587 (Bauschlicher et al., 1991; Fukuda, 2012)		
II	single Na ⁺ -H ₂ O (Mashkovtsev et al., 2016; Fukuda and Shinoda, 2008; Fukuda, 2012)		ν_2	bending (Charoy et al., 1996)	1631 (Fukuda and Shinoda, 2008; Fukuda et al., 2009)	E _{1c} (Charoy et al., 1996)	
					1633 (Mashkovtsev et al., 2016)		
					1638 (Bauschlicher et al., 1991; Fukuda, 2012)		
II	single Na ⁺ -H ₂ O (Mashkovtsev et al., 2016; Fukuda and Shinoda, 2008; Fukuda, 2012)		ν_3	asymmetric stretching (Viana et al., 2002b)	3660 (Mashkovtsev et al., 2016)	E _{1c} (Charoy et al., 1996)	
II	double H ₂ O-Na ⁺ -H ₂ O (Mashkovtsev et al., 2016; Fukuda and Shinoda, 2008; Fukuda, 2012)		ν_1	symmetric stretching (Viana et al., 2002b)	3602 (Fukuda and Shinoda, 2008; Fukuda et al., 2009)		
					3600 (Mashkovtsev et al., 2016)		
					3597 (Fukuda, 2012)		
					3592 (Wood and Nassau, 1968; Mashkovtsev and Lebedev, 1993)		
II	double H ₂ O-Na ⁺ -H ₂ O (Mashkovtsev et al., 2016; Fukuda and Shinoda, 2008; Fukuda, 2012)		ν_2	bending (Charoy et al., 1996)	1619 (Fukuda and Shinoda, 2008; Fukuda et al., 2009)		
					1620 (Mashkovtsev et al., 2016)		
					1628 (Wood and Nassau, 1968; Mashkovtsev and Lebedev, 1993; Fukuda, 2012)		

Table 4. Continued.

Molecule	Type	Coordination	Vibrational mode	Type of vibration	Wavenumber [cm ⁻¹]	Polarisation
III			ν_3	asymmetric stretching (Viana et al., 2002b)	3660 (Mashkovtsev et al., 2016) 3655 (Wood and Nassau, 1968; Mashkovtsev and Lebedev, 1993)	
			ν_1	symmetric stretching (Viana et al., 2002b)	3550 (Mashkovtsev and Lebedev, 1993) (assumed)	
			ν_2	bending (Charoy et al., 1996)	1604 (Mashkovtsev and Lebedev, 1993)	
			ν_3	asymmetric stretching (Viana et al., 2002b)	3704 (Mashkovtsev and Lebedev, 1993)	
H ₂ O	free	uncoordinated	ν_1	symmetric stretching	3657 (Kolesov and Geiger, 2000) 3652 (Wood and Nassau, 1967)	n/a
			ν_2	bending	1595 (Kolesov and Geiger, 2000; Wood and Nassau, 1967)	n/a
			ν_3	asymmetric stretching	3756 (Kolesov and Geiger, 2000; Wood and Nassau, 1967)	n/a

n/a – not applicable.

deficiencies as a result of the replacement of structural Al and Be by substitution with lower-valence ions in the octahedral and tetrahedral sites and has been shown to correlate with the amount of substitution (Auricchio et al., 1988; Charoy et al., 1996). The amount of alkalis in beryl can reach values of 7 wt %–14 wt % in igneous and hydrothermal beryl, respectively (Viana et al., 2002b). Since the alkali cation is positively charged, it interacts with the partial negative charge of the O atom in the H₂O molecule (dipole moment) and thereby causes the molecule to change its orientation and become type II H₂O (e.g. Aines and Rossman, 1984; Charoy et al., 1996; Mashkovtsev et al., 2016). Therefore, the presence and amount of this type of H₂O depend in turn on the presence and amount of alkali ions within the channels (Blak et al., 1982). This is supported by findings on alkali-free, synthetic beryl samples, which were shown to lack type II H₂O (Wood and Nassau, 1968). However, it is possible for one alkali cation to attract two H₂O molecules. Therefore, two further subtypes of type II H₂O are distinguished: singly coordinated type II H₂O, with only one H₂O molecule attracted by one cation, and doubly coordinated type II H₂O, in which two H₂O molecules surround one cation (Mashkovtsev et al., 2016). Although it is frequently reported that the ratio between alkalis and type II H₂O in beryl is 1 : 2, Charoy et al. (1996) found their alkali-poor samples to exceed this ratio stated for pegmatitic beryl. In addition, an exponential correlation between the Raman peak intensities ratio for the peaks at 3598 cm⁻¹ and 3607 to 3608 cm⁻¹, resulting from type II and type I H₂O, respectively (Hagemann et al., 1990; Karam-

pelas et al., 2019), and the amount of Na and K was shown to exist in emeralds from different localities (Huong et al., 2010; Häger et al., 2020; Hanser et al., 2022) as illustrated in Fig. 5. Yet, with the alkali content being related to the amount of substitution within beryl and the type II H₂O being related to the amount of alkali ions, the type II H₂O content is also indirectly dependent on the amount of substitution. Generally, the two types of H₂O can be seen in the region between 3200–3800 cm⁻¹ in which the stretching modes of the OH⁻ are observed (Viana et al., 2002b). Stretching vibrations refer to the vibrational changes in bond lengths, while bending vibrations describe changes in binding angles in a molecule. Both types of H₂O have different absorption peaks in the infrared which are often seen as doublets (Fukuda et al., 2009). However, for type I H₂O, the ν_1 is weaker than its ν_3 , whereas for type II H₂O, it is the opposite (Mashkovtsev et al., 2016). The same is true for the motions in Raman spectroscopy, in which ν_1 is stronger than ν_3 (Kolesov and Geiger, 2000). In addition to these stretching and bending vibrations, type I and type II H₂O molecules can undergo libration motions (Wood and Nassau, 1967). These librational modes have been suggested to interact with the primary vibrational modes of H₂O and, for instance, cause symmetrical bands around the bending mode at 1629 cm⁻¹ observed in the polarised Raman spectra of beryl (Hagemann et al., 1990). In addition, H₂O, double coordinated around Na, is thought to exhibit lower bending and higher stretching vibrations than singly coordinated H₂O (Bauschlicher et al., 1991; Fukuda, 2012). Furthermore, the energies of the different vi-

brational modes of H₂O in beryl differ from those of free H₂O molecules. While some authors find higher bending and lower stretching modes in beryl (Fukuda, 2012), the opposite correlation has also been observed. Wood and Nassau (1967) found the bending vibration of type I H₂O to be the same as for the free H₂O molecule but the symmetric stretching and two of the three peaks of the asymmetric stretching vibration triplet to be of lower wavenumbers. Regardless of the scenario, the differences are thought to be rooted in the charges surrounding the H₂O molecules within beryl (Wood and Nassau, 1967) and the electrostatic interactions between the H atoms of the H₂O molecules and the O atoms in the walls of the structural channels in beryl in particular (Fukuda, 2012).

Thermometric studies have shown that type I H₂O is released from the beryl crystal more readily and at lower temperatures than type II H₂O (Bidny et al., 2011; Fukuda and Shinoda, 2008). The dehydration speed was observed to be faster when Na was absent (Łodziński et al., 2005). Furthermore, type II H₂O is released in a stepwise process by doubly coordinated type II H₂O first being converted to singly coordinated type II H₂O during heating and subsequently being released from the crystal entirely (Fukuda and Shinoda, 2008; Fridrichová et al., 2015). Dehydration has been observed to take place once the H₂O molecules are unbound and uncoordinated and have reached a gas-like state (Aines and Rossman, 1984; Łodziński et al., 2005). Until the H₂O was eliminated from the mineral, this state was observed to be reversible (Aines and Rossman, 1984). The high temperatures needed to eliminate the H₂O from the structural channels of beryl are often attributed to a plugging effect caused by the H₂O molecules and alkali ions within the channels themselves (Charoy et al., 1996; Aurisicchio et al., 1988; Łodziński et al., 2005). In order to dehydrate beryl, the plugging cations must either move to the channel walls or to the 2*a* site or have to be completely expelled from the channels to allow H₂O to escape the crystal (Aines and Rossman, 1984). The reversibility of the gas-like state, as well as the high dehydration temperature, can also be observed in the unchanged type I and type II H₂O features in the spectra of Goldman et al. (1978) after heating. Likewise, no alteration to the H₂O peaks occurred after irradiation. Although cordierite is frequently used as a reference material for studies on beryl, its bands attributed to its type I and type II H₂O are not only less sharp (Aines and Rossman, 1984), but beryl also exhibits higher dehydration temperatures than cordierite (Charoy et al., 1996; Aines and Rossman, 1984). Hu and Lu (2020), however, observed dehydration of liquid inclusions within beryl after heating above 400 °C, supposedly via microscopic cracks in the samples. In a study by Fukuda and Shinoda (2008), the ν_3 mode of type I H₂O in beryl was not altered after dehydration experiments compared to the ν_1 and ν_2 modes of type II H₂O, which led the authors to conclude that the former mode is not dependent on the concentration of H₂O within beryl, whereas the latter are. However, Bidny et al. (2011) observed the intensity of the absorption lines of

type I H₂O to decrease more strongly than those of type II H₂O after annealing at 950 °C. Furthermore, the lattice parameters of alkali-rich beryl have been reported to decrease once H₂O is removed during heating (Łodziński et al., 2005). In addition, more recent heating experiments have shown the release of H₂O and other molecules or ions from the channel to lower the vibrational energy of Si within beryl, which can be seen as a frequency shift from 1151 to 1136 cm⁻¹ in infrared (Bidny et al., 2011). Similarly, a peak in the nearby region between 1175–1200 cm⁻¹ has been shown to shift depending on the type II H₂O content (Viana et al., 2002b). The authors claim the peak is caused by interactions of the silicate rings with the H₂O molecules within (Viana et al., 2002b). This contrasts previous studies in which the same shift was attributed to substitutions in the crystal structure of beryl (Aurisicchio et al., 1994).

In addition to these aforementioned two types of H₂O, several authors have suggested type III H₂O species exist in beryl (Fig. 6). Mashkovtsev and Lebedev (1993) have proposed a third type of H₂O, resulting from H₂O being coordinated with heavy alkali cations such as Cs⁺ or K⁺. However, according to the authors, the wavenumbers of type I and type III H₂O only slightly differ from each other, with resulting overlap of peaks and only two, instead of the expected three, bands being visible in the IR spectra (Mashkovtsev and Lebedev, 1993). This type III H₂O is thought to have the same orientation as type I H₂O. The authors argue that this is the result of the large heavy alkalis' radii, which cause greater distances between the heavy alkalis and the H₂O molecules they interact with (since they could only occupy adjacent 2*a* sites), thus also affecting the frequencies of these H₂O molecules to a lesser extent than would be expected for lighter alkalis (Mashkovtsev and Lebedev, 1993). Still, Hawthorne and Černý (1977) found the bond strength sum around Cs to be close to its ideal value in beryl, thus making it unnecessary for Cs ions to bind to any H₂O molecules in the channel. Moreover, though type II H₂O is coordinated with a nearby alkali cation (Wood and Nassau, 1967), it was found to not necessarily be located in the immediate vicinity of it (Mashkovtsev and Solntsev, 2002). Furthermore, a study by Charoy et al. (1996) found another population of H₂O at around 3235 cm⁻¹ that did not correspond to either type I or type II H₂O and the orientation of which was identified as parallel to the channel axis by the authors (Charoy et al., 1996). Type I H₂O was assumed to be one possible configuration for the H₂O molecules inside a low-sodic, low-hydrous aquamarine from Brazil. Nonetheless, the authors of this study also gave an alternative explanation, suggesting the H–H vector of the H₂O molecule exhibits an inclination, intermediate to those observed in type I and type II H₂O, of 38° to the *c* axis of beryl (Artioli et al., 1993). In their interpretation of the data obtained during a later neutron diffraction analysis on a highly sodic, highly hydrous beryl from Ireland, the same authors argue for a strongly inclined orientation with the H–H vector at 38° and one of the two possible

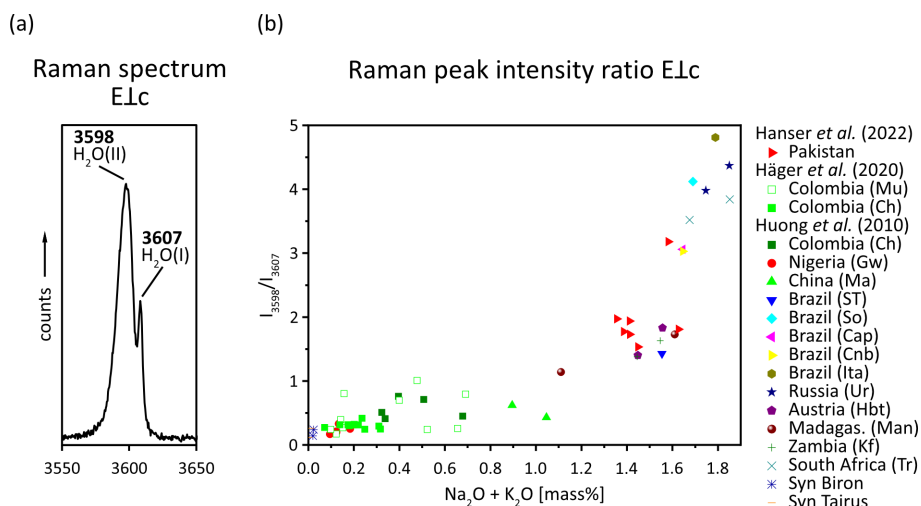


Figure 5. (a) Raman spectrum of an emerald from Chitral, Pakistan, in E_{1c} excitation showing Raman peaks caused by type I and type II H₂O (data from Hanser et al., 2022; the full Raman spectrum can be found therein). (b) The ratio between the type II H₂O peak and the type I H₂O peak against the Na₂O and K₂O contents for emeralds from different localities (modified after Huang et al., 2010; Häger et al., 2020; Hanser et al., 2022).

O–H vectors of H₂O being parallel to the *c* axis of the beryl crystal. This was thus proposed as a further possible way for H₂O molecules to be orientated within the channels of beryl (Artioli et al., 1995). Another type of H₂O, also referred to as type III H₂O, was proposed to be associated with Li present in beryl (Łodziński et al., 2005). The existence of Li coordinated with H₂O is supported by other authors and used to explain differing behaviour of H₂O in beryl (Mashkovtsev et al., 2016; Fukuda, 2012). While some authors found their type II H₂O spectra to be independent of the kind of alkali ion causing the orientation change of the H₂O molecule (Wood and Nassau, 1967), others observed lower bending and higher stretching vibrations when H₂O molecules were coordinated with a Li instead of a Na ion (Lee et al., 2004; Fukuda, 2012). Moreover, the substitution of Be²⁺ by lower-valence Li⁺ was proposed to be linked to H⁺ ions (Anderson, 2006). Furthermore, it was suggested that unbound H₂O was also present in the channels, with its symmetry axis being unaligned and thus randomly oriented (Łodziński et al., 2005). It has to be noted, however, that beryl can contain fluid inclusions (cavities with free H₂O in them), which may be measured alongside and thus influence the FTIR spectra.

Contrary to the idea of alkali ions in the channels of beryl compensating for charge imbalance by substitution of Al, Si or Be by lower-valence ions, Aurisicchio et al. (1988) proposed the presence of H₃O⁺ in the channels as charge deficiency compensators. Compared to this, the idea of hydroxyl groups forming hydroxides with alkali and earth alkaline metal ions in the channels of beryl (Wood and Nassau, 1967; Schmetzer and Kiefert, 1990) is more widely accepted. Protons were also suggested to act as charge compensators (Manier-Glavinaz et al., 1989; Andersson, 2006,

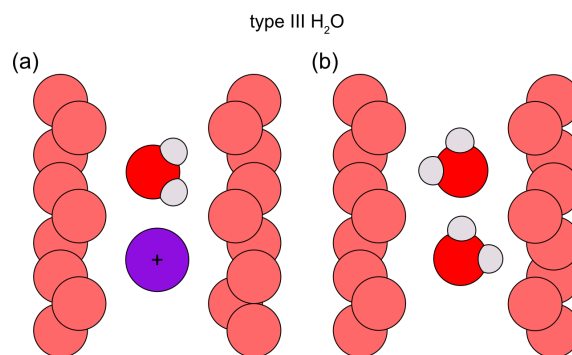


Figure 6. Proposed type III H₂O orientations. The channel wall O atoms are depicted in light red; the H₂O molecules are dark red and grey. (a) Type III H₂O (according to Mashkovtsev and Lebedev, 1993) coordinated with a heavy alkali, such as Cs (purple circle). The H₂O molecule has been proposed to have the same orientation as type I H₂O. The type III H₂O and the alkali each reside at a *2a* site, creating a larger distance between each other compared to H₂O and a lighter alkali. (b) Type III H₂O (according to Artioli et al., 1993, 1995) with one O–H vector parallel to and the H–H vector inclined by 38° with regard to the *c* axis of the crystal.

2019). These may, in turn, be attached to O atoms of the channel walls and thus form hydroxyl groups (Andersson, 2019).

In more recent studies the influence of H₂O on colour was investigated (Wang et al., 2022a, b). The authors found the unit cell parameters *a* and *b* to correlate with the amount of type II H₂O. Furthermore, they argued that Fe³⁺ in the channel and type II H₂O combined to form Fe hydrate, giving rise to a yellow colour and inducing a green hue in otherwise blue beryls. However, the change in unit cell parameters was

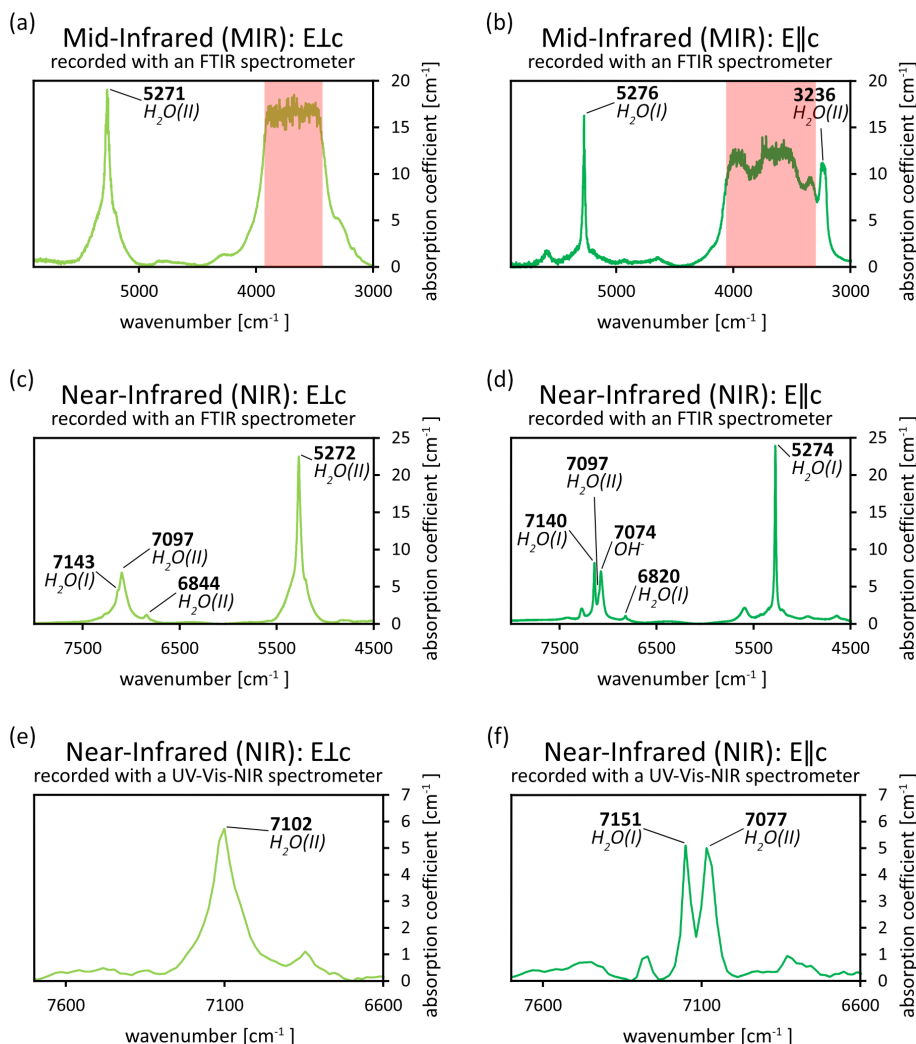


Figure 7. (a–f) Spectra of an emerald from Chitral, Pakistan, in the MIR and NIR ranges, recorded with FTIR and UV–Vis–NIR spectrometers (data from Hanser et al., 2022; full spectra can be found therein). Owing to the thickness of the sample, the MIR spectra (a–b) could not be resolved in the range relevant for H₂O absorption (red area). However, absorption related to type I and type II H₂O can be seen in the NIR range of the FTIR spectra (c–d) and the UV–Vis–NIR spectra (e–f) as overtone peaks (peak assignments according to Wood and Nassau, 1967; Mashkovtsev and Smirnov, 2004; Mashkovtsev et al., 2016). Please note that some assignments may vary depending on the literature.

previously shown to be rooted in the amount of substitution in beryl. As explained above, lower-valence substituting ions than the original constituting components (Al³⁺, Si⁴⁺, Be²⁺) would make charge compensation by cations, such as Na⁺, necessary (e.g. Aurisicchio et al., 1988; Charoy et al., 1996; Fridrichová et al., 2018; Andersson, 2019). The interaction of the cation with H₂O will then force it to become type II H₂O (e.g. Aines and Rossman, 1984; Charoy et al., 1996; Mashkovtsev et al., 2016). Hence, the correlation between the unit cell parameters and type II H₂O is indirect and the consequence of preceding processes. Furthermore, addressing Fe hydrates as a form of H₂O is inaccurate. Therefore, concluding that H₂O has an effect on the colour of beryl is misleading. In addition, as outlined above, the presence of Fe ions in the channels of beryl remains disputed.

Recording polarised FTIR spectra in the mid-infrared range for the detection of absorption by H₂O may pose a problem if samples are not thin enough. This is especially of concern for gemstones, for which a reduction of the sample thickness is not an option. The resulting signal overflow at the detector may not allow for the spectra to be resolvable. Figure 7 illustrates this phenomenon (see also Hanser et al., 2022). However, overtone peaks can be found in the near-infrared at twice the wavenumber of the principal vibrations and can thus confirm the presence of H₂O species. These absorptions can be recorded with FTIR and even some UV–Vis–NIR spectrometers. However, FTIR spectrometers generally have a higher sensitivity and spectral resolution for the infrared range than UV–Vis–NIR spectrometers, which can cause differences in peak positions when comparing spectra

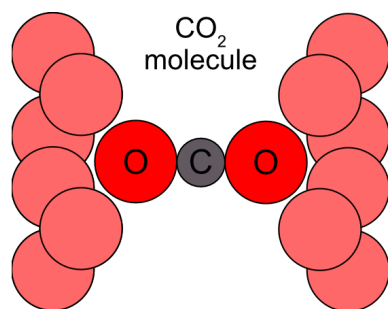


Figure 8. The orientation of the CO₂ molecule within the structural channels of beryl. The channel O atoms are depicted in light red. The CO₂ molecule resides in the 2*a* site and is orientated perpendicular to the *c* axis of the crystal (modified after Łodziński et al., 2005; Fukuda, 2012; Wang et al., 2021).

from both instruments. The presence of type II H₂O and its relative intensity compared to type I H₂O can also help in determining the geographic provenance of a sample (Hanser et al., 2023). The extreme case of no type I H₂O being detected with FTIR spectroscopy was shown to help in differentiating between natural and synthetic aquamarines (Adamo et al., 2008a).

4.3 CO₂

In contrast to H₂O, not all of the vibrational modes of CO₂ are IR-active. Therefore, all but the ν_1 mode of CO₂ can be seen in infrared as its vibrations corresponding to symmetric stretching are not IR-active (Charoy et al., 1996). Furthermore, owing to its large linear dimension, the CO₂ molecule occupies the 2*a* site in an orientation normal to the channel axis (Charoy et al., 1996; Gatta et al., 2006; Wood and Nassau, 1967) as shown in Fig. 8. The CO₂ molecule was assigned to the peak at 2360 cm⁻¹ in infrared. This absorption is observed as a strong peak in E \perp c (Fukuda, 2012). Still, in some studies, a small absorption was observed in the same region in E \parallel c as well (Gatta et al., 2006). However, this may also be caused by atmospheric CO₂ and thus represent an artefact (Gatta et al., 2006). Gatta et al. (2006) observed the peak at 2359 cm⁻¹ in a polarisation E \parallel a, whereas Łodziński et al. (2005) give a range of wavenumbers indicating the presence of CO₂ in beryl as 2361–2359 cm⁻¹. This CO₂-attributed absorption is shown in Fig. 9.

However, in Raman spectroscopy, the CO₂-specific peaks are located at 1240 cm⁻¹ (ν_1) and 1386 cm⁻¹ ($2\nu_2$) and are dependent on the polarisation direction being E \perp c for them to be visible, thus confirming the perpendicular orientation of the molecule with regard to the channel length and the *c* axis of the crystal (Charoy et al., 1996; Łodziński et al., 2005). Contrary to the H₂O content within the channels, the concentration of CO₂ was neither found to depend on the amount of alkali ions present nor found to be as easily expelled from the crystal as H₂O molecules since it was still

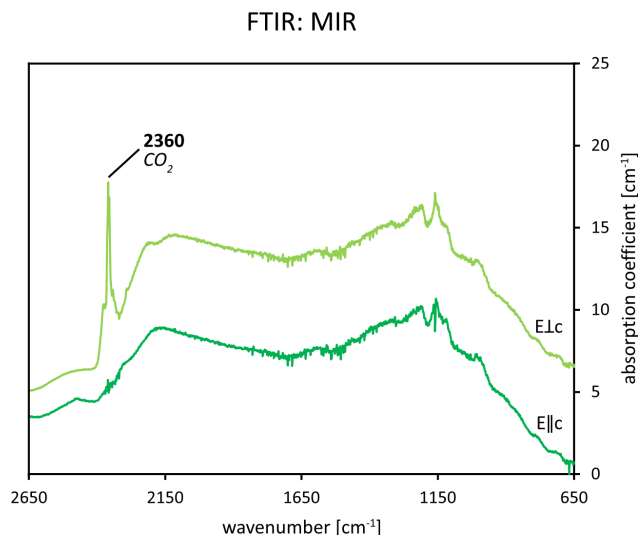


Figure 9. FTIR spectra of an emerald from Chitral, Pakistan, in the MIR range (data from Hanser et al., 2022; full spectra can be found therein). The sharp absorption at approximately 2360 cm⁻¹ in the E \perp c direction is attributed to CO₂. The traces are offset for clarity.

present in IR spectra during heating above 1000 °C (Łodziński et al., 2005). Still, the similar wavenumbers of CO₂ in the IR absorption spectra of beryl compared to those of the free CO₂ molecule have been proposed to reflect the weak interaction of the molecule with the surrounding structural channels of beryl (Łodziński et al., 2005).

5 Conclusions

Beryl is not only an interesting mineral for mineralogists and petrologists, but also forms an important group of gemstones for the gem market. As a result of multi-analysis studies, there is now a general consensus on the main features, such as the assignment of absorption bands to trace elements and foreign molecules. Therefore, optical absorption and vibrational spectroscopies have become useful, non-destructive tools to characterise beryl and allow the identification of the main colour-inducing trace elements like V, Cr, and Fe and the detection of further molecules possibly present in beryl, including H₂O. This can, in turn, help to determine the beryl variety, the possible geographic origin and to establish growth conditions or treatments, like the exposure to natural or artificial radiation. Nevertheless, there are other characteristics, the causes of which remain under debate or are still unknown (Table 5). This especially concerns the position, valence state and influence of Fe ions on the colour of beryl, as is reflected by the open debates on this topic in the literature. More advanced analysis techniques, such as transmission electron microscopy, electron paramagnetic resonance and Mössbauer spectroscopy, are expected to offer new insights for the study of beryl. However, they have not yet been

Table 5. Overview of the consensus and ongoing debates found in the literature.

Consensus			
Transition metal ions	Site	Colour induced	Variety
Mn	octahedral (Al)	pink and red	morganite and red beryl
V	octahedral (Al)	green	emerald
Cr	octahedral (Al)	green	emerald
Alkalis	Site	Comments	
Na	channel	to balance charge deficiency by substitution with lower-valence ions than original framework components	
Molecules	Site	Orientation	Comments
H ₂ O type I	channel	H–H vector parallel to the <i>c</i> axis of beryl	not coordinated with alkali
H ₂ O type II	channel	H–H vector perpendicular to the <i>c</i> axis of beryl	coordinated with alkali (Na)
CO ₂	channel	O–C–O perpendicular to the <i>c</i> axis of beryl	
Debates			
Transition metal ions	Site	Matter of debate	
Fe ²⁺	octahedral (Al)*	might be too large for coordination polyhedron* might not cause colour*	
	tetrahedral (Be)*	might be too large for coordination polyhedron* might not cause colour*	
	tetrahedral (Si)*	might be too large for coordination polyhedron*	
	interstitial (6g)*		
	channel*	might not enter channel* might induce blue colour*	
Fe ³⁺	octahedral (Al)	might not cause colour* might induce yellow colour*	
	tetrahedral (Be)*	might be too large for coordination polyhedron*	
	tetrahedral (Si)*	might be too large for coordination polyhedron*	
	interstitial (6g)*		
	channel*	might not enter channel* might induce yellow colour*	
Alkalis	Site	Matter of debate	
Li	tetrahedral*	direct substitution of Be* indirect substitution of Be (at interstitial tetrahedral site with tetrahedral Be site vacant)*	
	channel*	acting as charge balance*	
Molecules	Site	Orientation	Comments
H ₂ O type III*	channel*	same orientation as type II H ₂ O*	coordinated with Li*
	channel*	same orientation as type I H ₂ O*	coordinated with heavy alkali*
	channel**	H–H vector at 38° to <i>c</i> axis of beryl*	

* Still debated.

able to clarify all the remaining uncertainties and, thereby, fully settle the discussions. It must be considered that deductions made on samples of one beryl variety or from one location or occurrence only may not necessarily hold true for all others, as the growth environments and the subsequent availability of trace elements can differ. This also means that seemingly opposing theories are not necessarily mutually exclusive but might be based on samples which were subjected to different growth conditions. In these cases, broader studies with a wider variety of samples would be necessary to span a larger variability in trace element and H₂O contents. However, the availability of suitable specimens may pose a problem. This is especially true for questions concerning gem quality samples, for which non-destructive testing is usually an additional essential requirement.

Data availability. The original UV-Vis-NIR spectra shown in Fig. 3 are used for illustration purposes only. They are similar to spectra of the particular beryl varieties found in the literature. Requests for the data sets can be sent to the corresponding author. The Raman and FTIR spectra of the Chitral emerald shown in Figs. 5a, 7a–f and 9 were obtained from the authors of Hanser et al. (2022).

Author contributions. CSH acquired the UV-Vis-NIR spectra shown and prepared the initial manuscript. TH and RB supervised the project. All authors revised and commented on the manuscript.

Competing interests. The contact author has declared that none of the authors has any competing interests.

Disclaimer. Publisher's note: Copernicus Publications remains neutral with regard to jurisdictional claims made in the text, published maps, institutional affiliations, or any other geographical representation in this paper. While Copernicus Publications makes every effort to include appropriate place names, the final responsibility lies with the authors.

Acknowledgements. The authors would like to thank Qi Wang and Tom Stephan from the German Gemmological Association for supplying photos of gem quality beryl varieties. Furthermore, we thank Tom Stephan for his helpful comments on the manuscript.

Financial support. This open-access publication was funded by Johannes Gutenberg University Mainz.

Review statement. This paper was edited by Alessandro Pavese and reviewed by two anonymous referees.

References

- Adamo, I., Pavese, A., Prospero, L., Diella, V., Ajò, D., Gatta, G. D., and Smith, C. P.: Aquamarine, maxixe-type beryl, and hydrothermal synthetic blue beryl: analysis and identification, *Gems Gemol.*, 44, 214–226, 2008a.
- Adamo, I., Gatta, G. D., N. Rotiroti, Diella, V., and Pavese, A.: Gemmological investigation of a synthetic blue beryl: a multi-methodological study, *Mineral. Mag.*, 72, 799–808, <https://doi.org/10.1180/minmag.2008.072.3.799>, 2008b.
- Aines, R. D. and Rossman, G. R.: The high temperature behavior of water and carbon dioxide in cordierite and beryl, *Am. Mineral.*, 69, 319–327, 1984.
- Alkmim, D. G., de Almeida, F. O. T., and Lameiras, F. S.: FTIR study of aquamarines after gamma irradiation, heat treatment and electrodiffusion, *REM, Int. Eng. J.*, 70, 289–292, <https://doi.org/10.1590/0370-44672016700076>, 2017.
- Andersson, L. O.: The difference between maxixe beryl and maxixe-type beryl: an electron paramagnetic resonance investigation, *J. Gemm.*, 16, 313–317, 1979.
- Andersson, L. O.: The positions of H⁺, Li⁺ and Na⁺ impurities in beryl, *Phys. Chem. Miner.*, 33, 403–416, <https://doi.org/10.1007/s00269-006-0086-x>, 2006.
- Andersson, L. O.: EPR investigation of the methyl radical, the hydrogen atom and carbon oxide radicals in Maxixe-type beryl, *Phys. Chem. Miner.*, 35, 505–520, <https://doi.org/10.1007/s00269-008-0245-3>, 2008.
- Andersson, L. O.: EPR investigation of NO₂ and CO₂ – and other radicals in beryl, *Phys. Chem. Miner.*, 37, 435–451, <https://doi.org/10.1007/s00269-009-0345-8>, 2010.
- Andersson, L. O.: The yellow color center and trapped electrons in beryl, *Can. Mineral.*, 51, 15–25, <https://doi.org/10.3749/canmin.51.1.15>, 2013.
- Andersson, L. O.: Comments on Beryl Colors and on Other Observations Regarding Iron-containing Beryls, *Can. Mineral.*, 57, 551–566, <https://doi.org/10.3749/canmin.1900021>, 2019.
- Arivazhagan, V., Schmitz, F. D., Vullum, P. E., Van Helvoort, A. T. J., and Holst, B.: Atomic resolution imaging of beryl: an investigation of the nano-channel occupation: ATOMIC RESOLUTION IMAGING OF BERYL, *Journal of Microscopy*, 265, 245–250, <https://doi.org/10.1111/jmi.12493>, 2017.
- Artioli, G., Rinaldi, R., Stahl, K., and Zanazzi, P. F.: Structure refinements of beryl by single-crystal neutron and X-ray diffraction, *American Mineralogist*, 78, 762–768, 1993.
- Artioli, G., Rinaldi, R., Wilson, C. C., and Zanazzi, P. F.: Single-crystal pulsed neutron diffraction of a highly hydrous beryl, *Acta Crystallogr B Struct Sci*, 51, 733–737, <https://doi.org/10.1107/S0108768194014631>, 1995.
- Aurischio, C., Fioravanti, G., Grubessi, O., and Zanazzi, P. F.: Reappraisal of the crystal chemistry of beryl, *American Mineralogist*, 73, 826–837, 1988.
- Aurischio, C., Grubessi, O., and Zecchini, P.: Infrared spectroscopy and crystal chemistry of the beryl group, *Can. Mineral.*, 32, 55–68, 1994.
- Bakakin, V., Rylov, G., and Belov, N.: X-ray diffraction data for identification of beryl isomorphs, *Geochem. Int.*, 7, 1302–1311, 1970.
- Bauschlicher, C. W., Langhoff, S. R., Partridge, H., Rice, J. E., and Komornicki, A.: A theoretical study of Na(H₂O)_n⁺ (n = 1–4), *J.*

- Chem. Phys., 95, 5142–5148, <https://doi.org/10.1063/1.461682>, 1991.
- Belyanchikov, M. A., Zhukova, E. S., Tretiak, S., Zhugayevych, A., Dressel, M., Uhlig, F., Smiatek, J., Fyta, M., Thomas, V. G., and Gorshunov, B. P.: Vibrational states of nano-confined water molecules in beryl investigated by first-principles calculations and optical experiments, *Phys. Chem. Chem. Phys.*, 19, 30740–30748, <https://doi.org/10.1039/C7CP06472A>, 2017.
- Bersani, D., Azzi, G., Lambruschi, E., Barone, G., Mazzoleni, P., Raneri, S., Longobardo, U., and Lottici, P. P.: Characterization of emeralds by micro-Raman spectroscopy: Characterization of emeralds, *J. Raman Spectrosc.*, 45, 1293–1300, <https://doi.org/10.1002/jrs.4524>, 2014.
- Bidny, A. S., Baksheev, I. A., Popov, M. P., and Anosova, M. O.: Beryl from deposits of the Ural Emerald Belt, Russia: ICP-MS-LA and infrared spectroscopy study, *Moscow Univ. Geol. Bull.*, 66, 108–115, <https://doi.org/10.3103/S0145875211020037>, 2011.
- Blak, A. R., Isotani, S., and Watanabe, S.: Optical absorption and electron spin resonance in blue and green natural beryl, *Phys. Chem. Miner.*, 8, 161–166, <https://doi.org/10.1007/BF00308238>, 1982.
- Bragg, W. L. and West, J.: The structure of beryl, *Be₃Al₂Si₆O₁₈*, *P. Roy. Soc. Lond. A Mat.*, 111, 691–714, <https://doi.org/10.1098/rspa.1926.0088>, 1926.
- Bunnag, N., Kasri, B., Setwong, W., Sirisurawong, E., Chotsawat, M., Chirawatkul, P., and Saiyasombat, C.: Study of Fe ions in aquamarine and the effect of dichroism as seen using UV-Vis, NIR and x-ray, *Radiat. Phys. Chem.*, 177, 109107, <https://doi.org/10.1016/j.radphyschem.2020.109107>, 2020.
- Burns, R. G.: *Mineralogical applications of crystal field theory*, Cambridge University Press, ISBN 9780521430777, 1993.
- Chankhanttha, C., Thanasuthipitak, P., and Kidkhunthod, P.: Iron K-Edge Xanes Study of Heated Green Beryl from Madagascar, *Walailak Journal of Science and Technology (WJST)*, 13, 977–983, 2016.
- Charoy, B., de Donato, P., Barres, O., and Pinto-Coelho, C.: Channel occupancy in an alkali-poor beryl from Serra Branca (Goias, Brazil): spectroscopic characterization, *Am. Mineral.*, 81, 395–403, <https://doi.org/10.2138/am-1996-3-414>, 1996.
- de Almeida Sampaio Filho, H., Sighinolfi, G. P., and Galli, E.: Contribution to the crystal chemistry of beryl, *Contrib. Mineral. Petr.*, 38, 279–290, <https://doi.org/10.1007/BF00373593>, 1973.
- Dvir, M. and Low, W.: Paramagnetic Resonance and Optical Spectrum of Iron in Beryl, *Phys. Rev.*, 119, 1587–1591, <https://doi.org/10.1103/PhysRev.119.1587>, 1960.
- Edgar, A. and Vance, E. R.: Electron paramagnetic resonance, optical absorption, and magnetic circular dichroism studies of the CO₃²⁻ molecular-ion in irradiated natural beryl, *Phys. Chem. Miner.*, 1, 165–178, <https://doi.org/10.1007/BF00307316>, 1977.
- Figueiredo, M. O., Pereira da Silva, T., Veiga, J. P., Leal Gomes, C., and De Andrade, V.: The blue colouring of beryls from Licungo, Mozambique: an X-ray absorption spectroscopy study at the iron K-edge, *Mineral. Mag.*, 72, 175–178, <https://doi.org/10.1180/minmag.2008.072.1.175>, 2008.
- Fridrichová, J., Baěík, P., Rusinová, P., Antal, P., Škoda, R., Bizovská, V., and Miglierini, M.: Optical and crystal-chemical changes in aquamarines and yellow beryls from Thanh Hoa province, Vietnam induced by heat treatment, *Phys. Chem. Miner.*, 42, 287–302, <https://doi.org/10.1007/s00269-014-0719-4>, 2015.
- Fridrichová, J., Baěík, P., Ertl, A., Wildner, M., Dekan, J., and Miglierini, M.: Jahn-Teller distortion of Mn³⁺-occupied octahedra in red beryl from Utah indicated by optical spectroscopy, *J. Mol. Struct.*, 1152, 79–86, <https://doi.org/10.1016/j.molstruc.2017.09.081>, 2018.
- Fritsch, E. and Rossman, G. R.: An update on color in gems. Part 2: Colors involving multiple atoms and color centers, *Gems Gemol.*, 24, 3–15, 1988.
- Fukuda, J.: Water in Rocks and Minerals – Species, Distributions, and Temperature Dependences, in: *Infrared Spectroscopy – Materials Science, Engineering and Technology*, edited by: Theophanides, T., InTech, <https://doi.org/10.5772/35668>, 2012.
- Fukuda, J. and Shinoda, K.: Coordination of water molecules with Na⁺ cations in a beryl channel as determined by polarized IR spectroscopy, *Phys. Chem. Miner.*, 35, 347–357, <https://doi.org/10.1007/s00269-008-0228-4>, 2008.
- Fukuda, J., Shinoda, K., Nakashima, S., Miyoshi, N., and Aikawa, N.: Polarized infrared spectroscopic study of diffusion of water molecules along structure channels in beryl, *Am. Mineral.*, 94, 981–985, <https://doi.org/10.2138/am.2009.3124>, 2009.
- Gaite, J.-M., Izotov, V. V., Nikitin, S. I., and Prosvirnin, S. Y.: EPR and optical spectroscopy of impurities in two synthetic beryls, *Appl. Magn. Reson.*, 20, 307–315, <https://doi.org/10.1007/BF03162283>, 2001.
- Gatta, G. D., Nestola, F., Bromiley, G. D., and Mattauch, S.: The real topological configuration of the extra-framework content in alkali-poor beryl: A multi-methodological study, *Am. Mineral.*, 91, 29–34, <https://doi.org/10.2138/am.2006.1896>, 2006.
- Gatta, G. D., Adamo, I., Zullino, A., Gagliardi, V., Lorenzi, R., Rotiroli, N., Faldi, L., and Proserpi, L.: A Multi-Methodological Investigation of Natural and Synthetic Red Beryl Gemstones, *Minerals*, 12, 439, <https://doi.org/10.3390/min12040439>, 2022.
- Goldman, D. S., Rossman, G. R., and Parkin, K. M.: Channel constituents in beryl, *Phys. Chem. Miner.*, 3, 225–235, <https://doi.org/10.1007/BF00633572>, 1978.
- Groat, L. A. and Turner, D.: *Geology and mineralogy of gemstones*, First edition, Wiley, American Geophysical Union, Hoboken, NJ, Washington, D.C., Wiley, ISBN 978-1-119-29987-5, 2022.
- Groat, L. A., Giuliani, G., Marshall, D. D., and Turner, D.: Emerald deposits and occurrences: A review, *Ore Geol. Rev.*, 34, 87–112, <https://doi.org/10.1016/j.oregeorev.2007.09.003>, 2008.
- Groat, L. A., Rossman, G. R., Dyar, M. D., Turner, D., Piccoli, P. M. B., Schultz, A. J., and Ottolini, L.: Crystal chemistry of dark blue aquamarine from the true blue showing, Yukon territory, Canada, *Can. Mineral.*, 48, 597–613, <https://doi.org/10.3749/canmin.48.3.597>, 2010.
- Gübelin, E. J.: Gemological Characteristics of Pakistani Emeralds, in: *Emeralds of Pakistan: geology, gemology, and genesis*, Geological Survey of Pakistan; Van Nostrans Reinhold, Islamabad, Pakistan: New York, N.Y., 269 pp., 75–91, ISBN 0-442-30328-9, 1989.
- Hagemann, H., Lucken, A., Bill, H., Gysler-Sanz, J., and Stalder, H. A.: Polarized Raman spectra of beryl and bazzite, *Phys. Chem. Miner.*, 17, 395–401, <https://doi.org/10.1007/BF00212207>, 1990.
- Häger, T., Rojas-Agramonte, Y., Charros-Leal, F., Villalobos-Basler, J. D., Gonzalez-Pinzon, M. A., and Hauenberger, C.:

- Smaragde aus Kolumbien, *Z. Dt. Gemmol. Ges.*, 69, 47–58, 2020.
- Hänni, H.: Blue-green Emerald from Nigeria (A consideration of terminology), *Australian Gemmologist*, 28, 16–17, 1992.
- Hanser, C. S., Gul, B., Häger, T., and Botcharnikov, R.: Emerald from the Chitral Region, Pakistan: A New Deposit, *Journal of Gemmology*, 38, 234–252, <https://doi.org/10.15506/JoG.2022.38.3.234>, 2022.
- Hanser, C. S., Stephan, T., Gul, B., Häger, T., and Botcharnikov, R.: Comparison of Emeralds from the Chitral District, Pakistan, with other Pakistani and Afghan Emeralds, *Journal of Gemmology*, 38, 582–599, <https://doi.org/10.15506/JoG.2023.38.6.582>, 2023.
- Hawthorne, F. and Černý, P.: The alkali-metal positions in Cs-Li beryl, *Can. Mineral.*, 15, 414–421, 1977.
- Hawthorne, F. C. and Huminicki, D. M. C.: The Crystal Chemistry of Beryllium, *Rev. Miner. Geochem.*, 50, 333–403, <https://doi.org/10.2138/rmg.2002.50.9>, 2002.
- Hu, Y. and Lu, R.: Color Characteristics of Blue to Yellow Beryl from Multiple Origins, *Gems Gemol.*, 56, 54–65, <https://doi.org/10.5741/GEMS.56.1.54>, 2020.
- Huong, L. T.-T., Häger, T., and Hofmeister, W.: Confocal micro-Raman spectroscopy: a powerful tool to identify natural and synthetic emeralds, *Gems Gemol.*, 46, 36–41, 2010.
- Jehlička, J., Culka, A., Bersani, D., and Vandenebeele, P.: Comparison of seven portable Raman spectrometers: beryl as a case study: Beryl identification by portable Raman instruments, *J. Raman Spectrosc.*, 48, 1289–1299, <https://doi.org/10.1002/jrs.5214>, 2017.
- Karampelas, S., Al-Shaybani, B., Mohamed, F., Sangsawong, S., and Al-Alawi, A.: Emeralds from the Most Important Occurrences: Chemical and Spectroscopic Data, *Minerals*, 9, 561, <https://doi.org/10.3390/min9090561>, 2019.
- Khaleel, F. M., Saleh, G. M., Lasheen, E. S. R., and Lentz, D. R.: Occurrences and genesis of emerald and other beryls mineralization in Egypt: A review, *Phys. Chem. Earth*, 128, 103266, <https://doi.org/10.1016/j.pce.2022.103266>, 2022.
- Kimble, F. S. and Haynes, P. E.: An occurrence of red beryl in the Black Range, New Mexico, *New Mexico Geology*, 2, 15–16, <https://doi.org/10.58799/NMG-v2n1.15>, 1980.
- Kolesov, B.: Vibrational states of H₂O in beryl: physical aspects, *Phys. Chem. Miner.*, 35, 271–278, <https://doi.org/10.1007/s00269-008-0220-z>, 2008.
- Kolesov, B. A. and Geiger, C. A.: The orientation and vibrational states of H₂O in synthetic alkali-free beryl, *Phys. Chem. Miner.*, 27, 557–564, <https://doi.org/10.1007/s002690000102>, 2000.
- Krambrock, K., Pinheiro, M. V. B., Guedes, K. J., Medeiros, S. M., Schweizer, S., Castañeda, C., Botelho, N. F., and Pedrosa-Souares, A. C.: Radiation-induced centers in Cs-rich beryl studied by magnetic resonance, infrared and optical spectroscopy, *Nucl. Instrum. Meth. B*, 191, 285–290, [https://doi.org/10.1016/S0168-583X\(02\)00577-3](https://doi.org/10.1016/S0168-583X(02)00577-3), 2002.
- Krzemnicki, M., Cartier, L., Lefèvre, P., and Zhou, W.: Colour varieties of gems—Where to set the boundary, *InColor*, 45, 92–95, 2020.
- Krzemnicki, M. S., Wang, H. A. O., and Büche, S.: A New Type of Emerald from Afghanistan's Panjshir Valley, *J. Gemmol.*, 37, 474–495, <https://doi.org/10.15506/JoG.2021.37.5.474>, 2021.
- Lambruschi, E., Gatta, G. D., Adamo, I., Bersani, D., Salvioli-Mariani, E., and Lottici, P. P.: Raman and structural comparison between the new gemstone pezzottaite Cs(Be₂Li)Al₂Si₆O₁₈ and Cs-beryl, *J. Raman Spectrosc.*, 45, 993–999, <https://doi.org/10.1002/jrs.4479>, 2014.
- Laurs, B. M., Simmons, W. B., Rossman, G. R., Quinn, E. P., McClure, S. F., Peretti, A., Armbruster, T., Hawthorne, F., Falster, A. U., Günther, D., Cooper, M. A., and Grobéty, B.: Pezzottaite from ambatovita, madagascar: a new gem mineral, *Gems Gemol.*, 39, 284–301, 2003.
- Lee, H. M., Tarakeshwar, P., Park, J., Kołaski, M. R., Yoon, Y. J., Yi, H.-B., Kim, W. Y., and Kim, K. S.: Insights into the Structures, Energetics, and Vibrations of Monovalent Cation-(Water)_{1–6} Clusters, *J. Phys. Chem. A*, 108, 2949–2958, <https://doi.org/10.1021/jp0369241>, 2004.
- Lin, J., Chen, N., Huang, D., and Pan, Y.: Iron pairs in beryl: New insights from electron paramagnetic resonance, synchrotron X-ray absorption spectroscopy, and ab initio calculations, *Am. Mineral.*, 98, 1745–1753, <https://doi.org/10.2138/am.2013.4472>, 2013.
- Lind, T. and Stephan, T.: Spektrentypen und Farben von eisen- und manganhaltigen Beryllen, *Z. Dt. Gemmol. Ges.*, 71, 27–40, 2022.
- Łodziński, M., Sitarz, M., Stec, K., Kozanecki, M., Fojud, Z., and Jurga, S.: ICP, IR, Raman, NMR investigations of beryls from pegmatites of the Sudety Mts, *J. Mol. Struct.*, 744–747, 1005–1015, <https://doi.org/10.1016/j.molstruc.2004.12.042>, 2005.
- Manier-Glavinaz, V., Couty, R., and Lagache, M.: The removal of alkalis from beryl; structural adjustments, *Can. Mineral.*, 27, 663–671, 1989.
- Mashkovtsev, R. I. and Lebedev, A. S.: Infrared spectroscopy of water in beryl, *J. Struct. Chem.*, 33, 930–933, <https://doi.org/10.1007/BF00745616>, 1993.
- Mashkovtsev, R. I. and Smirnov, S. Z.: The nature of channel constituents in hydrothermal synthetic emerald, *J. Gemmol.*, 29, 215–227, <https://doi.org/10.15506/JoG.2004.29.4.215>, 2004.
- Mashkovtsev, R. I. and Solntsev, V. P.: Channel constituents in synthetic beryl: ammonium, *Phys. Chem. Miner.*, 29, 65–71, <https://doi.org/10.1007/s002690100206>, 2002.
- Mashkovtsev, R. I. and Thomas, V. G.: Nitrogen atoms encased in cavities within the beryl structure as candidates for qubits, *Appl. Magn. Reson.*, 28, 401–409, <https://doi.org/10.1007/BF03166771>, 2005.
- Mashkovtsev, R. I., Thomas, V. G., Fursenko, D. A., Zhukova, E. S., Uskov, V. V., and Gorshunov, B. P.: FTIR spectroscopy of D₂O and HDO molecules in the *c*-axis channels of synthetic beryl, *Am. Mineral.*, 101, 175–180, <https://doi.org/10.2138/am-2016-5432>, 2016.
- Mathew, G., Karanth, R. V., Rao, T. K. G., and Deshpande, R. S.: Colouration in Natural Beryls: A Spectroscopic Investigation, *J. Geol. Soc. India*, 56, 285–303, 2000.
- McManus, C. E., McMillan, N. J., Harmon, R. S., Whitmore, R. C., De Lucia Jr., F. C., and Miziolek, A. W.: Use of laser induced breakdown spectroscopy in the determination of gem provenance: beryls, *Appl. Optics*, 47, G72, <https://doi.org/10.1364/AO.47.000G72>, 2008.
- McMillan, N. J., McManus, C. E., Harmon, R. S., De Lucia, F. C., and Miziolek, A. W.: Laser-induced breakdown spectroscopy analysis of complex silicate minerals—beryl, *Anal. Bioanal. Chem.*, 385, 263–271, <https://doi.org/10.1007/s00216-006-0374-9>, 2006.

- Mihalynuk, M. and Lett, R.: Composition of Logtung Beryl (aquamarine) by ICPE/MS: A Comparison with Beryl Worldwide, British Columbia Geological Survey, Geological Fieldwork 2003, 141–146, 2003.
- Mittani, J. C. R., Watanabe, S., Chubaci, J. F. D., Baptista, D. L., and Zawislak, F. C.: Ion beam modification of colorless silicates of beryl, *Surf. Coat. Tech.*, 158–159, 708–711, [https://doi.org/10.1016/S0257-8972\(02\)00252-9](https://doi.org/10.1016/S0257-8972(02)00252-9), 2002a.
- Mittani, J. C. R., Watanabe, S., Chubaci, J. F. D., Matsuoka, M., Baptista, D. L., and Zawislak, F. C.: γ -Radiation effects on colourless silicates of beryl, *Nucl. Instrum. Meth. B*, 191, 281–284, [https://doi.org/10.1016/S0168-583X\(02\)00576-1](https://doi.org/10.1016/S0168-583X(02)00576-1), 2002b.
- Mittani, J. C. R., Watanabe, S., Matsuoka, M., Baptista, D. L., and Zawislak, F. C.: Doping by diffusion and implantation of V, Cr, Mn and Fe ions in uncoloured beryl crystals, *Nucl. Instrum. Meth. B*, 218, 255–258, <https://doi.org/10.1016/j.nimb.2003.12.023>, 2004.
- Mokhtar, H., Surour, A. A., Azer, M. K., Ren, M., and Said, A.: New insights into chemical and spectroscopic characterization of beryl mineralization related to leucogranites in the west Wadi El Gemal area, southern Eastern Desert of Egypt, *Geochemistry*, 125980, <https://doi.org/10.1016/j.chemer.2023.125980>, 2023.
- Morosin, B.: Structure and thermal expansion of beryl, *Acta Crystallogr B Struct Crystallogr. Cryst. Chem.*, 28, 1899–1903, <https://doi.org/10.1107/S0567740872005199>, 1972.
- Nassau, K.: The origins of color in minerals, *Am. Mineral.*, 63, 219–229, 1978.
- Nassau, K.: Gemstone enhancement: history, science, and state of the art, St. Oxford and London (Butterworth Heinemann), 252 pp., 1994.
- Nassau, K. and Wood, D.: The nature of the new Maxixe-type beryl, *Lapidary Journal*, 27, 1032–1034, 1973.
- Nassau, K. and Wood, D. L.: An examination of red beryl from Utah, *Am. Mineral.*, 53, 801–806, 1968.
- Nassau, K., Prescott, B. E., and Wood, D. L.: The deep blue Maxixe-type color center in beryl, *Am. Mineral.*, 61, 100–107, 1976.
- Parkin, K. M., Loeffler, B. M., and Burns, R. G.: Mössbauer spectra of kyanite, aquamarine, and cordierite showing intervalence charge transfer, *Phys. Chem. Miner.*, 1, 301–311, <https://doi.org/10.1007/BF00307569>, 1977.
- Pecherskaya, S. G., Mikhailov, M. A., Demina, T. V., Bogdanova, L. A., and Belozerova, O. Yu.: Symmetry and ordering of compounds with a beryl-type structure in the Mg-enriched part of the beryllium indialite-cordierite-beryl system, *Crystallogr. Rep.*, 48, 363–369, <https://doi.org/10.1134/1.1578115>, 2003.
- Pieczka, A., Szełęg, E., Szuszkiewicz, A., Gołębiewska, B., Zelek, S., Ilnicki, S., Nejbart, K., and Turniak, K.: Cs-Bearing Beryl Evolving To Pezzottaite From the Julianna Pegmatitic System, SW Poland, *Can. Mineral.*, 54, 115–124, <https://doi.org/10.3749/canmin.1500075>, 2016.
- Platonov, A., Khomenko, V., and Taran, M.: Crystal Chemistry, Optical Spectra and Color of Beryl. I. Heliodor and Golden Beryl – Two Varieties of Natural Yellow Beryl, *Mineralogical Journal*, 38, 3–14, <https://doi.org/10.15407/mineraljournal.38.02.003>, 2016.
- Price, D. C., Vance, E. R., Smith, G., Edgar, A., and Dickson, B. L.: Mössbauer effect studies of beryl, *J. Phys. Colloques*, 37, C6-811–C6-817, <https://doi.org/10.1051/jphyscol:19766171>, 1976.
- Pøikryl, J., Novák, M., Filip, J., Gadas, P., and Galiová, M. V.: Iron+magnesium-bearing beryl from granitic pegmatites: an EMPA, LA-ICP-MS, Mössbauer spectroscopy, and powder xrd study, *Can. Mineral.*, 52, 271–284, <https://doi.org/10.3749/canmin.52.2.271>, 2014.
- Rudnick, R. L. and Gao, S.: Composition of the Continental Crust, in: *Treatise on Geochemistry*, Elsevier, 1–64, <https://doi.org/10.1016/B0-08-043751-6/03016-4>, 2003.
- Saeseaw, S., Renfro, N. D., Palke, A. C., Sun, Z., and McClure, S. F.: Geographic Origin Determination of Emerald, *Gems Gemol.*, 55, 614–646, <https://doi.org/10.5741/GEMS.55.4.614>, 2019.
- Schmetzer, K. and Kiefert, L.: Water in beryl – a contribution to the separability of natural and synthetic emeralds by infrared spectroscopy, *J. Gemm.*, 22, 215–223, <https://doi.org/10.15506/JoG.1990.22.4.215>, 1990.
- Schwarz, D., Kanis, J., and Kinnaird, J.: Emerald and green beryl from Central Nigeria, *Journal of Gemmology*, 25, 117–141, 1996.
- Shang, Y., Guo, Y., and Tang, J.: Spectroscopy and chromaticity characterization of yellow to light-blue iron-containing beryl, *Sci. Rep.*, 12, 10765, <https://doi.org/10.1038/s41598-022-11916-z>, 2022.
- Shannon, R. D.: Revised effective ionic radii and systematic studies of interatomic distances in halides and chalcogenides, *Acta Crystallogr. A*, 32, 751–767, <https://doi.org/10.1107/S0567739476001551>, 1976.
- Sherriff, B., Grundy, H. D., Hartman, J. S., Hawthorne, F., and P. Ěerný: The incorporation of alkalis in beryl; a multinuclear MAS NMR and crystal-structure study, *Can. Mineral.*, 29, 271–285, 1991.
- Skvortsova, V., Mironova-Ulmane, N., Trinkler, L., and Merkulov, V.: Optical Properties of Natural and Synthetic Beryl Crystals, *IOP Conference Series: Materials Science and Engineering*, 77, 012034, <https://doi.org/10.1088/1757-899x/77/1/012034>, 2015.
- Solntsev, V. P., Tsvetkov, E. G., Alimpiev, A. I., and Mashkovtsev, R. I.: Valent state and coordination of cobalt Ions in beryl and chrysoberyl crystals, *Phys. Chem. Miner.*, 31, 1–11, <https://doi.org/10.1007/s00269-003-0363-x>, 2004.
- Stephan, T., Häger, T., Henn, U., and Hofmeister, W.: The influence of V3+ on the colour of rubies and emeralds, shown by spectral fitting of UV/Vis/NIR absorption spectra, *Z. Dt. Gemmol. Ges.*, 68, 53–57, 2019.
- Taran, M. N. and Vyshnevskiy, O. A.: Be, Fe2+-substitution in natural beryl: an optical absorption spectroscopy study, *Phys. Chem. Miner.*, 46, 795–806, <https://doi.org/10.1007/s00269-019-01040-2>, 2019.
- Uher, P., Chudík, P., Baèik, P., Vaculoviè, T., and Galiová, M.: Beryl composition and evolution trends: an example from granitic pegmatites of the beryl-columbite subtype, Western Carpathians, Slovakia, *J. Geosci.*, 55, 69–80, <https://doi.org/10.3190/jgeosci.060>, 2012.
- Viana, R. R., da Costa, G. M., De Grave, E., Stern, W. B., and Jordt-Evangelista, H.: Characterization of beryl (aquamarine variety) by Mössbauer spectroscopy, *Phys. Chem. Miner.*, 29, 78–86, <https://doi.org/10.1007/s002690100210>, 2002a.
- Viana, R. R., Jordt-Evangelista, H., da Costa, G. M., and Stern, W. B.: Characterization of beryl (aquamarine variety) from pegmatites of Minas Gerais, Brazil, *Phys. Chem. Miner.*, 29, 668–679, <https://doi.org/10.1007/s00269-002-0278-y>, 2002b.

- Wang, H., Shu, T., Chen, J., and Guo, Y.: Characteristics of Channel-Water in Blue-Green Beryl and Its Influence on Colour, *Crystals*, 12, 435, <https://doi.org/10.3390/cryst12030435>, 2022a.
- Wang, H., Guan, Q., Liu, Y., and Guo, Y.: Effects of Transition Metal Ions on the Colour of Blue-Green Beryl, *Minerals*, 12, 86, <https://doi.org/10.3390/min12010086>, 2022b.
- Wang, P., Gray, T. P., Li, Z., Anderson, E. J. D., Allaz, J., Smyth, J. R., Koenig, A. E., Qi, L., Zhou, Y., and Raschke, M. B.: Mineralogical classification and crystal water characterisation of beryl from the W–Sn–Be occurrence of Xuebaoding, Sichuan province, western China, *Mineral. Mag.*, 85, 172–188, <https://doi.org/10.1180/mgm.2021.13>, 2021.
- Wood, D. L. and Nassau, K.: Infrared Spectra of Foreign Molecules in Beryl, *J. Chem. Phys.*, 47, 2220–2228, <https://doi.org/10.1063/1.1703295>, 1967.
- Wood, D. L. and Nassau, K.: The characterization of beryl and emerald by visible and infrared absorption spectroscopy, *Am. Mineral.*, 53, 777–800, 1968.
- Yu, X., Hu, D., Niu, X., and Kang, W.: Infrared Spectroscopic Characteristics and Ionic Occupations in Crystalline Tunneling System of Yellow Beryl, *JOM-J. Min. Met. Mat. S.*, 69, 704–712, <https://doi.org/10.1007/s11837-017-2266-1>, 2017.
- Zoltai, T.: Classification of silicates and other minerals with tetrahedral structures, *Am. Mineral.*, 45, 960–973, 1960.